Isotopically labeled ozone: a new approach to elucidate the formation of ozonation products

Millaray Sierra Olea[a], Simon Kölle[a], Emil Bein[a], Thorsten Reemtsma[b,c], Oliver J. Lechtenfeld[b,d], and Uwe Hübner[a*]

[a] Chair of Urban Water Systems Engineering, Technical University of Munich, Am Coulombwall 3, D-85748 Garching, Germany

[b] Department of Analytical Chemistry, Helmholtz Centre for Environmental Research – UFZ, Permoserstrasse 15, 04318 Leipzig, Germany

[c] Institute of Analytical Chemistry, University of Leipzig, Linnéstrasse 3, 04103 Leipzig, Germany

[d] ProVIS–Centre for Chemical Microscopy, Helmholtz Centre for Environmental Research–UFZ, Permoserstrasse 15, 04318 Leipzig, Germany

* Corresponding author: Chair of Urban Water Systems Engineering, Technical University of Munich, Am Coulombwall 3, D-85748 Garching, Germany

E-mail: u.huebner@tum.de (U. Hübner)

Abstract

As ozonation becomes a widespread treatment for removal of trace organic chemicals in wastewater treatment plant effluents, there are increasing concerns regarding the formation of ozonation transformation products (OPs), and their possible impacts on the aquatic environment and eventually human health. In this study, a novel method was developed that utilizes the heavy oxygen isotope (^{18}O) for the production of heavy ozone ($[^{18}O_1]O_2$, $[^{18}O_2]O_1$, $[^{18}O_3]$) to actively label OPs from oxygen transfer reactions. To establish and validate this new approach, venlafaxine with a well-described oxygen transfer reaction (tertiary amine -> N-oxide) was chosen as a model compound. Observed $^{18}O/^{16}O$ ratios in the major OP venlafaxine N-oxide (NOV) correlated with expected ^{18}O purities based on previous tracer experiments. These results confirmed the successful labeling with heavy oxygen and furthermore demonstrate the potential to monitor NOV as an indicator of $^{18}O/^{16}O$ ratios during ozonation. As a next step, $^{18}O/^{16}O$ ratios were used to elucidate the formation mechanism of previously described OPs from sulfamethoxazole (SMX). Seven OPs were detected including the frequently described nitro-SMX, which was formed with a maximum yield of 3.2% (of initial SMX). With the successful labeling of six of the seven OPs from sulfamethoxazole, it was possible to confirm their previously proposed formation pathways, and distinguish oxygen transfer

from electron transfer reactions. OPs $^{18}O/^{16}O$ ratios indicate that hydroxylation of the aromatic ring and formation of nitro-groups mostly follows oxygen transfer reactions, while electron transfer reactions initiate the formation of hydroxylamine and the abstraction of NH_2 leading to catechol.

Keywords: ozonation products, oxygen-18, isotope labeling, wastewater

1. Introduction

Chemicals of Emerging Concern (CECs) have their origin in our daily domestic and industrial applications (Loos et al., 2013; Margot et al., 2013). The main concern with CECs is related to their biologically active design and wide range of application (Lee and Von Gunten, 2016). Their high polarity and poor degradability (high persistence) prevents the efficient removal in conventional WWTPs (Reemtsma et al., 2006), which results in constant discharge into surface waters at detectable concentrations (ng L^{-1} to µg L^{-1}) (Margot et al., 2013; Ternes et al., 2003). Ozonation is an advanced treatment technology currently used in wastewater treatment plants (WWTPs) to reduce the concentrations of CECs in their discharged effluent (Bourgin et al., 2018; Eggen et al., 2014; Gulde et al., 2021; Huber et al., 2005; Margot et al., 2013; Ternes et al., 2003). Despite the known benefits of ozone for oxidation, which often leads to immediate loss of biological activity (e.g., hormones, antibiotics) (Huber et al., 2004) there are still uncertainties regarding the transformation of CECs into a mix of unknown and potentially hazardous ozonation products (OPs) (Hübner et al., 2015; Lee and Von Gunten, 2016; Wert et al., 2007).

OPs are formed by the partial oxidation of compounds when they react with ozone (von Gunten, 2003; Von Sonntag and Von Gunten, 2012). The selective reaction of ozone often results in a limited number of major OPs (Lim et al., 2019; Zucker et al., 2018), with their formation controlled by the reactive functional groups in the parent compound (Tentscher et al., 2019). In contrast, diffusion dependent reactions with hydroxyl radicals (•OH), that are generated as secondary oxidants from ozone reactions with the water matrix, form numerous OPs at low individual concentration (von Gunten, 2003).

With the current understanding of ozone reaction mechanisms, examples of OPs formation from parent functional groups, are: N-oxides and dealkylated products formed from tertiary amines, nitroalkanes and or hydroxylamines formed from aliphatic primary and secondary amines, hydroxylated compounds formed from aromatic scaffolds, as well as, aldehydes and ketones formed from unsaturated carbons chains (Lee and Von Gunten, 2016; Lim et al., 2019; Tekle-Röttering et al., 2016; Zucker et al., 2018). Knowledge gaps still exist for ozonation reaction kinetics and mechanisms for Sulfur (S) and Nitrogen (N) containing moieties. In S- containing moieties (thiols, thioethers, and disulfides), the formation of a sulfoxide (SO) has been proposed as the most common functional group (Dodd et al., 2010), but only limited knowledge about the possible subsequent reactions to form sulfone (SO_2), sulfonic acid (SO_3H), and sulfate (SO_4^{2-}) is available (Lim et al., 2022). For N- containing moieties, there is uncertainty in the case of secondary amines, where, although hydroxylamines were suggested as a major product, studies have shown that this might be only an intermediate and nitro-alkanes are the major OP (Lim et al., 2022).

In previous experiments focused on drinking water treatment, the use of isotopically labeled (^{13}C, ^{15}N and ^{2}H) parent compounds facilitated the identification of reaction sites for ozone, as well as, the elucidation of the formed OPs by their characteristic isotopic pattern (Brunner et al., 2019; Kolkman et al., 2015; Liu et al., 2019; Spahr et al., 2015; Spahr et al., 2017). The use of labeled compounds (^{13}C, ^{14}C, ^{15}N and ^{2}H) has also been applied to study different CECs and their OPs kinetics and formation pathways in WWTP (Betsholtz et al., 2022; Borowska et al., 2016; Dodd and Huang, 2004; Mawhinney et al., 2012; Willach et al., 2017). These studies have focused on particular compounds considered relevant, either by their abundance or by their toxicity, but were not based on the reactivity of the specific functional groups with ozone. Because of the overwhelming number of CECs and organic matter in wastewater, rather than evaluating every single compound and its OPs in a complex mixture, it is more efficient to generate transferable knowledge regarding individual functional group reactivity with ozone and the expected OPs (von Gunten, 2018).

The objective of this study is to establish and validate a novel isotope labeling method by using isotopically labeled ozone ($[^{18}O]_3$) to oxidize selected model compounds and produce isotopically labeled OPs. The method has been validated by the ozonation of a model substance (Venlafaxine) with well-known reaction mechanism with ozone (tertiary amine -> N-oxide), and then applied to investigate the reaction mechanism of

sulfamethoxazole (sulfonamide) leading to formation of 4-nitro-sulfamethoxazole and other OPs. By using this approach, we put emphasis on functional group reactivity towards ozone. This alternative approach can supply information such as reaction site/preference when more than one functional group is present, explicit reaction mechanism and reaction pathway for OPs formation, and enable the detection of OPs and ozonation by-products (OBPs) formed during ozonation of complex wastewater or drinking water matrices. In a parallel study, we successfully implemented our new concept for the detection of OBPs during the ozonation of effluent organic matter (EfOM) (Jennings et al., under review). The results from this study demonstrate that labeling of the OPs allows extrapolation of knowledge to more complex scenarios.

2. Materials and Methods

2.1. Chemicals and reagents

For sample preparation, the following compounds were used: venlafaxine hydrochloride (VLX), sulfamethoxazole (SMX) primidone (PRI), and tert-butanol (t-BuOH, ≥99 %). Technical O_2 and N_2 gases were used for initial testing of the system. Heavy oxygen gas ($^{18}O_2$ ≥97%) was used for the production of labeled ozone. Additional information regarding the chemicals and gases used can be found in the SI, Table S 1.

2.2. Generation of labeled ozone stock solution

Configuration of the ozonation system. A previously established ozonation system (Müller et al., 2019) was modified with the addition of two gas feedlines ($^{18}O_2$, N_2) and the positioning of 2- and 3-way valves (SI, Figure S 1). These modifications allow the system to be operated as a closed-circuit with the possibility of recovering the used gas from the experiments. A bellows pump (5 NL min^{-1}) was used to maintain and guarantee the gas flow inside the system. For gas conditioning, two water traps with molecular sieve 3 Å were placed before the ozone generator. The reactor volume was 500 mL and a needle valve port was implemented for the controlled extraction of the ozone stock solution. For additional information regarding the components of the system, refer to SI Table S 2.

Determination of mixing ratios using N_2 and O_2 gases. To simulate mixing and concentration of gases, tracer tests with N_2 and O_2 gases were conducted to determine optimum times for operating (opening and closing) of the gas lines, as well as, establishing the optimal conditions of gas pressure and flow. The test was performed by initially saturating the system with 100% O_2 gas until stable reading in an inline oxygen sensor. Subsequently, the two valves controlling O_2 and N_2 were simultaneously closed and opened, respectively. Finally, after a pre-determined amount of time, the valve controlling the system mode (open circuit vs. gas recirculation) was closed. The breakthrough curves obtained from the shift from 100 % O_2 to N_2 as well as the final mixing ratios were monitored in the inline oxygen sensor.

Generation of the ozone solution. Technical O_2 gas and $^{18}O_2$ (≥97%) gas were used as input-gas for the ozone generator BMT 803 BT. The ozone gas was continuously bubbled in the reactor, which was filled with ultrapure water and cooled in an ice-filled container (~4°C). Required volumes of ozone stock solution (to set a concentration of approximately 25 mg L^{-1}) were extracted from the reactor using a gastight glass syringe. This volume was used to determine the dissolved ozone concentration in the stock solution and for the ozonation of the samples. The dissolved ozone concentration was measured by the colorimetric indigo carmine method (Bader, 1982).

2.3. Batch ozonation experiments

Sample preparation. Samples for batch experiments with VLX and VLX/SMX were prepared in separate 20 mL vials. To elucidate the reaction mechanism of ozone with model compounds, the formed hydroxyl radicals (•OH) were scavenged by using t-BuOH with a k_{OH} 6 x 10^8 M^{-1} s^{-1} (Von Sonntag and Von Gunten, 2012). The necessary concentrations of t-BuOH for the experiments with VLX and VLX/SMX were adjusted according to Willach et al. (2017). To corroborate the efficiency of the scavenging agent, primidone with a k_{O3} 1 M^{-1} s^{-1} and k_{OH} 6.7 x 10^9 M^{-1} s^{-1} (Real et al., 2009) was used as a radical indicator. In parallel, samples without t-BuOH were prepared. All samples for ozonation were prepared in phosphate buffer at pH 7. A detailed composition for each batch experiment is given in SI, Table S 3.

Ozonation experiments. To establish the labeling method and validate its performance, initial experiments with VLX as sole ozone reactive compound were performed. As

reported by Zucker et al. (2018), the major ozonation product of venlafaxine is venlafaxine-N-oxide (NOV). The reaction mechanism of this compound proceeds by the transfer of one oxygen atom from the ozone molecule to the nitrogen of the tertiary amine functional group (SI, Figure S 3). Alternative transformation reactions (i.e., N-dealkylation, ozone attack at the activated aromatic ring) were not considered since they were only expected to affect the yield of NOV but not its $^{18}O/^{16}O$ ratio.

Consequently, a total of six experiments were performed. Three experiments were completed with VLX as sole reactive compound: first with technical ^{16}O gas, and two experiments with the different times previously characterized for the change of the gas lines at 0.5 bar (9 sec and 17 sec). In these batch experiments 20 µmol L^{-1} of VLX was oxidized using ozone dosages of 20 - 100 µmol L^{-1}. Subsequently, three additional experiments were performed at 0.9 bar with adjusted times for the gas line change according to breakthrough curves experiments (13 sec and 21 sec). One experiment was of VLX as sole reactive to corroborate the impact of pressure in the expected ^{18}O purity. The approach of labeling of OPs with ^{18}O was then applied to investigate transformation reactions for SMX. Samples containing a 1:5 molar ratio of VLX/SMX (10 µmol L^{-1} VLX, and 50 µmol L^{-1} SMX) were prepared and oxidized with ozone dosages of 50 - 300 µmol L^{-1}. A list of the targeted molar ratios for both compounds can be found in SI, Table S 4. The volume in all experiments was adjusted to 10 mL and samples were stored at 4°C until measurement.

2.4. Sample analysis

Compound quantification. Samples were measured on an LC-MS/MS (PLATINblue UHPLC – Knauer, Germany, ABSciex TQUAD 6500 – SCIEX, USA), using a method established and described by Müller et al. (2017). Quantification of VLX, venlafaxine N-oxide (NOV), SMX and PRI was accomplished in positive MRM (multiple reaction monitoring) mode. The quantification of the OPs 4-nitro sulfamethoxazole (NIT), was performed in negative MRM mode. To determine the $^{18}O/^{16}O$ ratio in labeled NOV and NIT, the qualifying and quantifying fragments´ *m/z* values were modified to include the expected labeling site and mass shift. For additional information regarding Q1 and Q3 masses and internal standards, refer to SI, Table S 5.

Separation and detection of SMX OPs. The separation of the OPs from SMX was performed with a Waters XSelect HSS T3 column (100Å, 3.5 µm, 2.1 mm x 100 mm,

Waters Germany) on an LC-MS system (Agilent 1260 Infinity – Agilent Technologies, USA, ABSciex Qtrap 5500 - SCIEX, USA). For the separation of the compounds, a gradient method was developed (SI, Table S 6). The solvents used were, ultrapure water (Arium Pro, Sartorius AG, Göttingen, Germany) and acetonitrile (hypergrade for LC-MS, LiChrosolv, Merck KGaA, Darmstadt, Germany) supplemented with 0.1% formic acid (LC-MS grade, HiPerSolv, VWR Chemicals, Leuven, Belgium). For compound detection in negative mode, Enhanced MS Scan (EMS) and Enhanced Product Ion Scan (EPI) were applied. The mass ranges used in both scan types can be found in SI, Table S 7. Data exploration and integration of the peak areas was performed with the software Analyst 1.6.2 (ABSciex - SCIEX, USA).

2.5. Data handling and calculations

Analysis of SMX OPs. For the integration of peak areas of the labeled SMX OPs, isotopologue fractions (IF) for the monoisotopic mass and the integration of up to two labeled oxygen atoms were determined according to Mairinger and Hann (2020). The MS^1 scans of individual samples and their isotopologue peaks were analyzed focusing on their centroid mass (Da), peak start (Da) and peak end (Da). Mean and standard deviation of discrete *m/z* ranges were used to define the starting and ending values for the different isotopic distribution of the isotopologues (SI, Table S 8). Once discrete and nonoverlapping *m/z* ranges were determined, isotopologue peak areas with M+0 ([^{16}O], 2[^{16}O]), M+2 Da ([^{18}O]) and M+4 Da (2[^{18}O]) were integrated (SI, Table S 9). It should be noted that these calculations were performed by evaluating MS^1 data with low resolution.

Oxygen transfer reaction probabilities. The $^{18}O/^{16}O$ ratios determined in the formed NOV (from single oxygen transfer reaction to VLX) were applied to elucidate the formation pathway of OPs from SMX. These $^{18}O/^{16}O$ ratios were used to calculate the expected isotopologue fractions during the formation of SMX OPs with two oxygen additions (eq. 1), where *x* and *y* denote the number of ^{16}O and ^{18}O atoms and Pr(^{16}O) and Pr(^{18}O) represent the probabilities determined by VLX measurements (modified from Valkenborg et al. (2012)).

$$Pr\left(^{16}O_x\ ^{18}O_y\right) = \frac{(x+y)!}{x! \times y!} \Pr\left(^{16}O\right)^x \times \Pr\left(^{18}O\right)^y \quad (1)$$

However, this calculated isotopologue distribution does not yet consider the natural isotopologues of the parent molecule. The web platform *enviPat* (Loos et al., 2015)

was used to predict the expected isotopic pattern of SMX + 2O, and the relative abundance of relevant natural isotopologues (monoisotopic mass [M], M+2) (SI, Text S 1). As an example, the calculated distribution of SMX-OPs with and without consideration of natural isotopologues are illustrated in Figure 1 for assumed probabilities of ^{18}O (Pr(^{18}O)) of 0%, 30% and 90%. Results indicate a limited effect of the natural isotopologues on the distribution of ^{18}O-OPs from SMX, but this might become different for ozonation of larger molecules, especially when they contain several sulfur atoms. These hypothetical values were then contrasted with the empirical results obtained from signal intensities of SMX OPs.

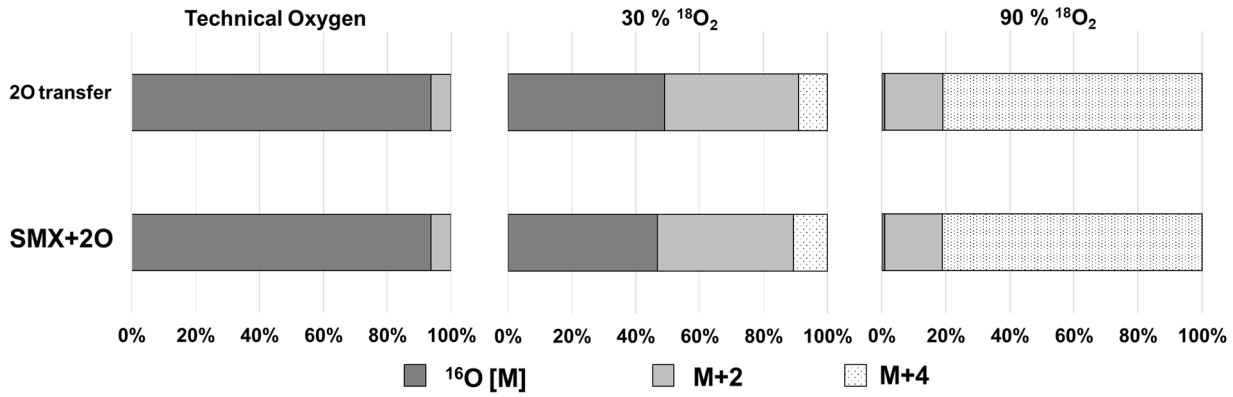

Figure 1. Example calculation of the expected isotopologue fractions (IF) of an SMX-OPs from two oxygen transfer reactions with and without consideration of relevant natural isotopologues (^{13}C, ^{15}N, ^{33}S, ^{34}S, ^{36}S, ^{17}O, ^{18}O) from SMX. Results show hypothetical distributions for ozonation with ozone from technical oxygen (^{16}O), 30% ^{18}O and 90% ^{18}O.

3. Results and Discussion

3.1. Method development and validation

The establishment and validation of the novel labeling method was performed as follows: (1) evaluation of N_2 and O_2 gas mixing ratios, (2) quantification of the $^{18}O/^{16}O$ ratio in NOV, and (3) correlation of the gas mixing ratios with labeling success of NOV. Following this approach, we were able to confirm the suitability of VLX to indicate the $^{18}O/^{16}O$ of OPs from oxygen transfer reactions.

Determination of mixing ratios using N_2 and O_2 gases. The purity of $^{18}O_2$ depends on the gas loading time (seconds), which is the duration of gas feeding from the $^{18}O_2$ container before the ozonation system is changed to recirculation mode. We simulated

$^{18}O_2$ purity by exchanging O_2 with N_2. Initially, nine different gas loading times were tested during operation at 0.5 bar generator pressure in replicate experiments (minimum 2 to up to 17 replicates for most promising settings) and gas loading times were compared with regards to their mixing ratios (simulated purity of $^{18}O_2$), and the volume of gas that could not be recovered for future experiments (Figure 2A). Since an increase in gas loading times beyond 17 s did not considerably improve gas purity to values >90 %, this operational setting was selected for experiment with highest purity of labeled ozone production (91.4%). In addition, experiments with 9 s were conducted to obtain the lowest purity of $^{18}O_2$.

After slight modifications of the ozone system (increased volume from additional dehumidification, higher generator pressure of 0.9 bar), experiments were repeated with slightly different gas loading times of 13 s and 21 s. Two example breakthrough curves are shown in Figure 2B. Results demonstrate that full breakthrough is reached after approximately 30 - 40 s, followed by several minutes of oscillation in the recirculated system until both gases are fully mixed. In addition, the green arrow in Figure 2B demonstrates the impact of pressure on the oxygen sensor, as the 20% increase in O_2 gas can only be explained by a pressure change in the system after switching from gas feeding to recirculation (see SI, Text S 2 for details). Also the type of gas being exchanged (O_2 to N_2 vs N_2 to O_2) seems to affect the results (SI, Figure S 2).

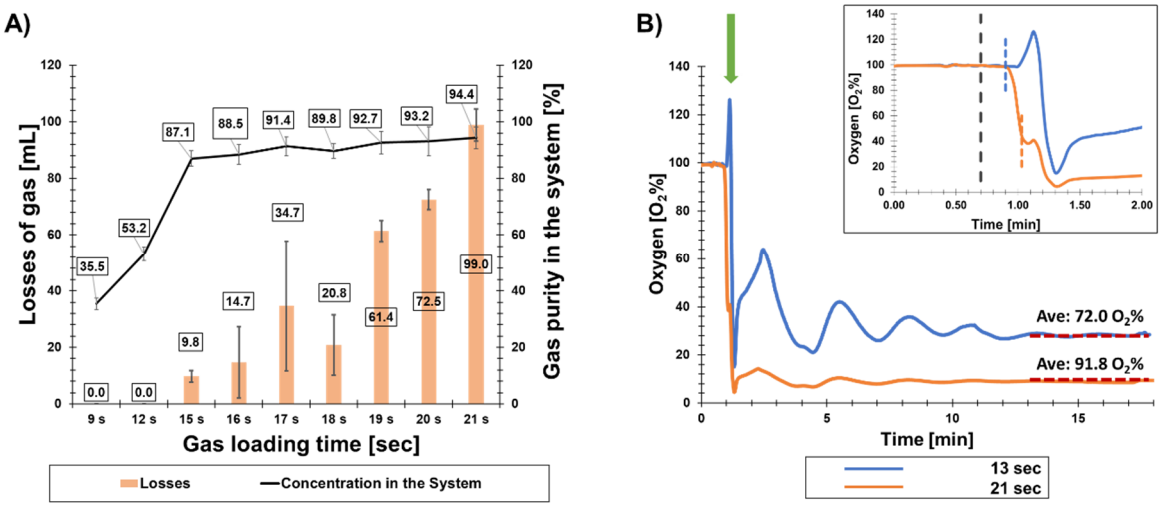

Figure 2. (**A**) The purity of $^{18}O_2$ that is expected depending on the gas loading times, as well as, the volume of gas that would be purged in each of the tested times. Error bars indicate standard deviation from variable number of replicates (2 - 27) at different times. (**B**) Breakthrough curve observed in the experiments for determination of system

settings and $^{18}O_2$ purity determination. The inlet shows the first 2 min with the dotted black line indicating the change of gas lines, the dotted blue and orange lines the times the system was closed.

Determination of $^{18}O/^{16}O$ ratios using NOV. With the operational protocol established, the expected ^{18}O gas purity simulated with the tracer N_2/O_2 experiments were corroborated by performing heavy ozone experiments and using the ozonation product NOV of VLX as indicator of labeling success. As a reference for the isotope distribution of OP formed by ozonation, the relative ion intensity of NOV in an experiment with $^{16}O_3$ was quantified (97 % *m/z* 294 $[M+H]^+$ and 3 % *m/z* 296 $[M+H]^+$). This isotope pattern was additionally compared with the values obtained from the calculation performed by using the *enviPat* platform (Loos et al., 2015) (SI, Text S 3). Because these samples were analyzed with an MRM method, with modified Q1 and Q3 masses that considered the labeled fragment, other possible isotopologues were not measured.

In the ozonation experiments with different $^{18}O/^{16}O$ ratios, the oxygen transfer reaction was confirmed by the changes in the relative abundance of the isotopic fraction of the detected peaks ([M+0], [M+2]) of the produced NOV molecule (Figure 3A). Therefore, when comparing the values for *m/z* 294 $[M+H]^+$ and *m/z* 296 $[M+H]^+$ obtained in the $^{16}O_3$ experiments, with the results observed in the produced NOV *m/z* of the different $^{18}O/^{16}O$ ozone experiments, the labeling success was reflected in the results, where the highest labeling success was 79 ± 1% ^{18}O-NOV, meanwhile the lowest was 43.9 ± 0.3% ^{18}O-NOV. The results of these experiments show that the $^{18}O/^{16}O$ ratios of the labeled NOV are stable and independent of the removed VLX, and ozone concentration dosed.

Additionally, as shown in Figure 3B, the $^{18}O/^{16}O$ ratio of labeled NOV changed according to the simulated concentrations of $^{18}O_2$ (O_2/N_2 ratio) in the system. Increasing the proportion of heavy oxygen in the ozonation system, increased the proportion of the heavy-labeled transformation product (^{18}O-NOV). The correlation between both variables was found to be $R^2 = 0.9605$, which indicates that ^{18}O-NOV formation is a suitable proxy for the estimation of the $^{18}O/^{16}O$ ratio.

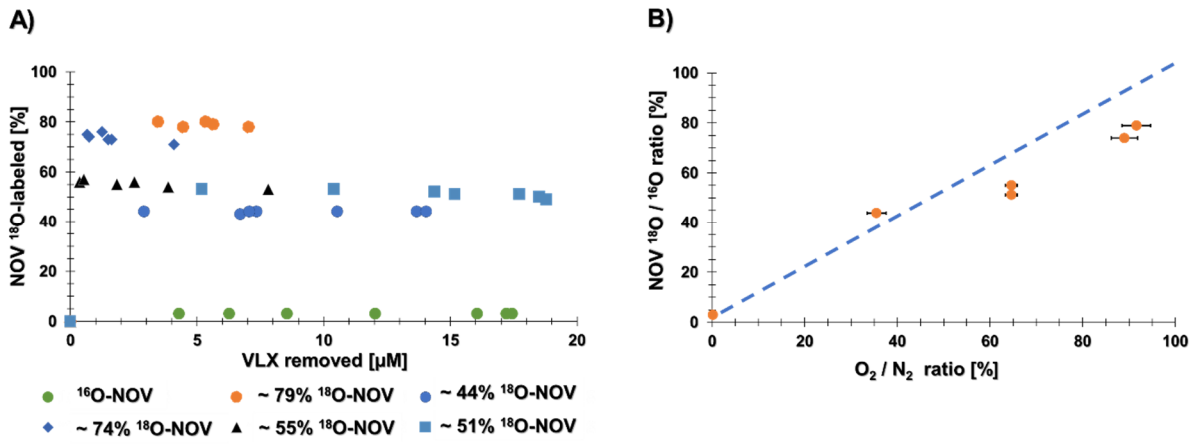

Figure 3. (**A**) Labeling of NOV depending on the $^{18}O/^{16}O$ ratios applied in the ozonation experiments with different ^{18}O purities (**B**) the relative intensity of the ions of interest for the experiments with a range of different $^{18}O_3/^{16}O_3$ concentrations compared to expected ratios from N_2/O_2 experiments.

However, as can be seen in Figure 3B the labeling success has an observable scattering that can be explained by different factors. First, the system is operated by a human and the changing of the gas lines must be done in seconds, thus any millisecond delay or mistake will considerably impact the gas purity. Second, the estimation of the oxygen percentage depends on the pressure in the gas line (see Figure 2A), therefore a higher reading of the oxygen sensor should be taken into consideration. Third, two different purities of $^{18}O_2$ were used for the production of ozone, the first had a purity of 99 ^{18}O% (Sigma-Aldrich, USA), the second 97 ^{18}O% (Linde GmbH, Germany). Fourth, the isotope kinetic effect of the four possible isotopologues of ozone is unknown, indicating some uncertainty regarding their individual reaction rates with VLX. Notwithstanding, the changes in the isotopic pattern, the formed NOV is produced by the change in the abundance of ^{16}O and ^{18}O in the system and the labeling of this compound with ^{18}O will therefore be used as a surrogate to establish $^{18}O/^{16}O$ ratios during following experiments with other compounds and matrices.

3.2. Sulfamethoxazole pathway elucidation

Quantification and semi-quantification of SMX OPs. In experiments with ^{16}O-ozone, six OPs were separated and detected (Figure 4). These products were previously reported in other studies, providing MS data and possible formation pathways (Gao et al., 2014;

Gómez-Ramos et al., 2011; Willach et al., 2017). Additionally, it was possible to detect a seventh previously unreported OP, OP284. To confirm the chemical identity of OP282a, the commercially available standard for 4-nitro-sulfamethoxazole (NIT) was used, this also enabled its quantification (SI, Figure S 5). The yield of NIT produced was 3.2 ± 0.3 % when the removal of SMX was 99.8 ±0.2 % (SI, Figure S 6). These values are within the previously 10% reported by Tekle-Röttering et al. (2016) for total product yield of nitrobenzene, nitrosobenzene and azobenzene, although in our work it was not possible to detect the formation of nitroso or azo sulfamethoxazole OPs. Additionally, there was no significant difference in the removal of SMX and the formation of labeled NIT, regardless of the $^{18}O/^{16}O$ ratio used for the production of the labeled ozone.

Peak areas (counts) of the seven OPs can be found in SI, Figure S 7. There, the formation of the OPs is illustrated as a function of the SMX removal. The comparison of cumulative intensities from isotopologues (IF) with results from ozonation with technical oxygen does not show any systematic deviation that would indicate different behavior of ozonation with different $^{18}O_2$ abundances.

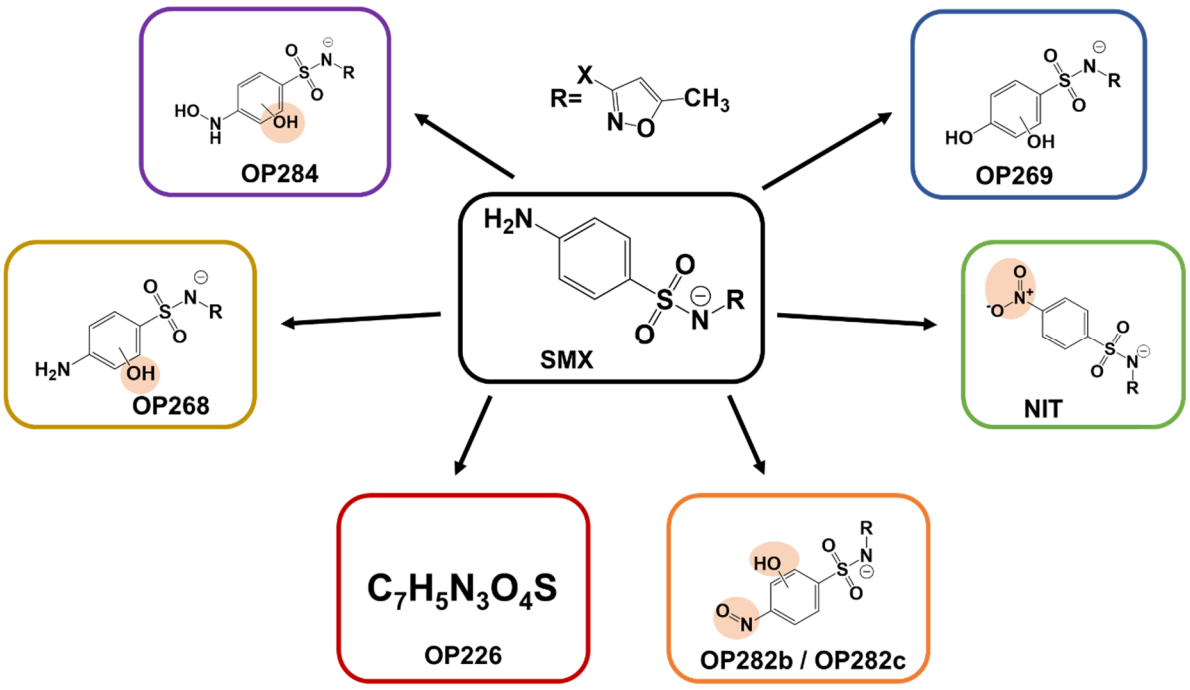

Figure 4. Detected OPs from SMX with proposed structures assigned based on previous studies (orange circles highlight the formed functional group with oxygen-18 added to the molecule, numbers indicate *m/z* in negative mode).

Application of $^{18}O/^{16}O$ ratios in VLX/SMX ozonation. Figure 5 illustrates measured isotopologue distributions for all detected SMX-OPs in comparison to the expected distribution for transfer of one oxygen (indicated by NOV distribution) and the expected probabilities for two oxygen transfer reactions (shown as 2O transfer).

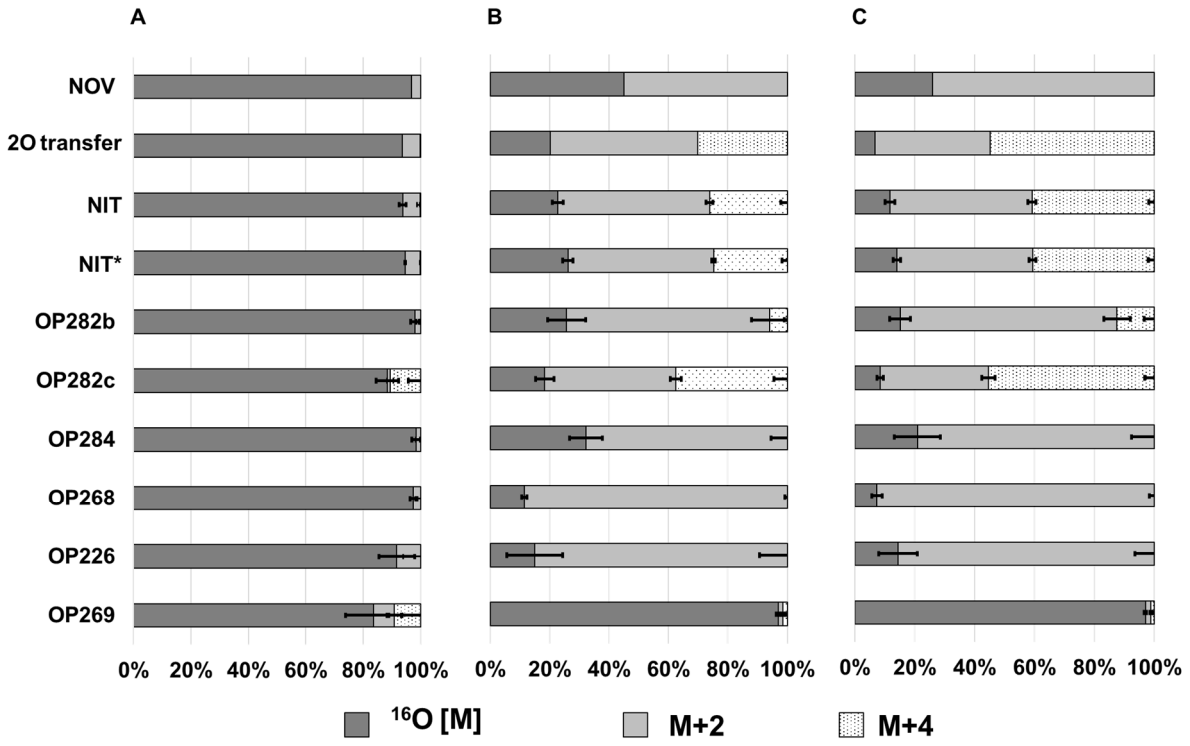

Figure 5. Change of the isotopologue distribution in the formation of different SMX OPs. OPs obtained from ozonation with technical oxygen (**A**) are compared to OPs obtained from ozone with a 55 ± 1.5 % ^{18}O purity (**B**) and 74 ± 1.3 % ^{18}O purity (**C**) based on NOV measurements (NIT* was quantified by MRM using the transitions *m/z* 282/186, *m/z* 284/188 and *m/z* 286/190, while all other isotopologue distributions were derived from the intensity of the respective molecular ions). Error bars indicate standard deviation observed in the formation of labeled OPs being produced by different ozone dosages.

Six of the seven detected OPs from SMX showed a shift in their monoisotopic peak area and isotopologue fraction, aligning with the measured NOV $^{18}O/^{16}O$ ratio. These shifts in the isotopic pattern of the ion indicate the successful addition of one or two ^{18}O atoms during ozonation. As can be seen in Figure 5, the three isomers of *m/z* 282 (NIT, OP282b and OP282c) seemed to be a result of two oxygen transfer reactions from the labeled ozone. Isotopologue distributions of NIT were determined from integration of qualitative MS^1 data (shown as NIT) and from MRM quantification (NIT*). Overall, results show a good agreement between both analytical methods, indicating

that MS^1 data is suitable to assess isotopologue distribution for other OPs without an available standard. Minor differences, although significant (p-value < 0.05) when comparing between the measurements of the isotopologues fractions of NIT (*m/z* 282, 284 and 286) and the results obtained from the integration of the fragments of interest in (OP282NIT*) (*m/z* 282/186, *m/z* 284/188 and *m/z* 286/190 of the 55 %$^{18}O_2$), can be explained by the higher selectivity of the MRM method and the different criteria used for the data integration. OPs 282b and 282c showed stronger deviation from expected distribution for 2O transfer reactions. Occurrence of the *m/z* 286 isotopologue of OP282c after ozonation with $^{16}O_3$ indicates co-elution of a different molecule at the same retention time, which can explain the shift in all experiments. In contrast, limited formation of *m/z* 286 for OP282b might be related to competing reactions of the intermediate, e.g. parallel oxidation by ozone and dissolved oxygen.

The formation of OP284, OP268, and OP226 can be explained by one oxygen transfer reaction (Figure 5). The observed deviation in their ^{18}O content from the value expected from NOV may be due to their low peak areas. While OP268 and OP226 are solely generated through oxygen transfer reaction, OP284 contains an additional oxygen, which was not derived from ozone. Lastly, OP269 is the single OP not being formed by a direct oxygen transfer reaction from the labeled ozone despite the addition of 2 oxygen atoms during the reaction. The direct reaction of O_3 with the aromatic ring or nitrogen functional group has been proposed as formation pathway for several of the reported OPs of SMX (Gao et al., 2014; Gómez-Ramos et al., 2011; Willach et al., 2017). However, the ^{18}O-labelling approach developed in this study is the first to prove the origin of the oxygen in the ozonation products. This illustrates how ^{18}O-labeling gives additional insight into the mechanism and transformation pathways during ozonation.

Elucidation of ozone reaction pathways. For the formation of NIT, two different formation pathways were proposed by Willach et al. (2017). Pathway A (reaction (1)-(3)) in Figure 6 was proposed based on the reaction of ozone as an H-abstractor with the formation of a radical pair, a subsequent cage reaction and release of water (Tekle-Röttering et al., 2016). Pathway B (reaction (4)-(6)) was proposed based on the insertion reaction of ozone at the nitrogen, where the intermediate would release a hydroperoxyl radical and form a nitroxyl radical, which would decay assisted by water once again forming sulfamethoxazole and 4-nitro sulfamethoxazole (Von Sonntag and Von Gunten, 2012). A third alternative, formation pathway C, was proposed by Yu et

al. (2017) by using density functional theory (DFT). They proposed a hydrogen atom transfer (HAT) mechanism as the first step, producing an amino radical and a •OOOH radical, which would recombine with the amino radical. This newly formed intermediate could have its H_2O_2 replaced by ozone, releasing O_2 and forming the nitro group (reaction (7)-(12)). These three previously proposed pathways have in common that the two transferred oxygen atoms originate from the ozone molecule. This agrees with the results obtained from the labeling experiments, where both transferred oxygen atoms are labeled according to the expected $^{18}O/^{16}O$ ratios. Therefore, it is not possible to distinguish based on probabilities, which one of these three pathways (Figure 6) is responsible for the formation of the nitro group.

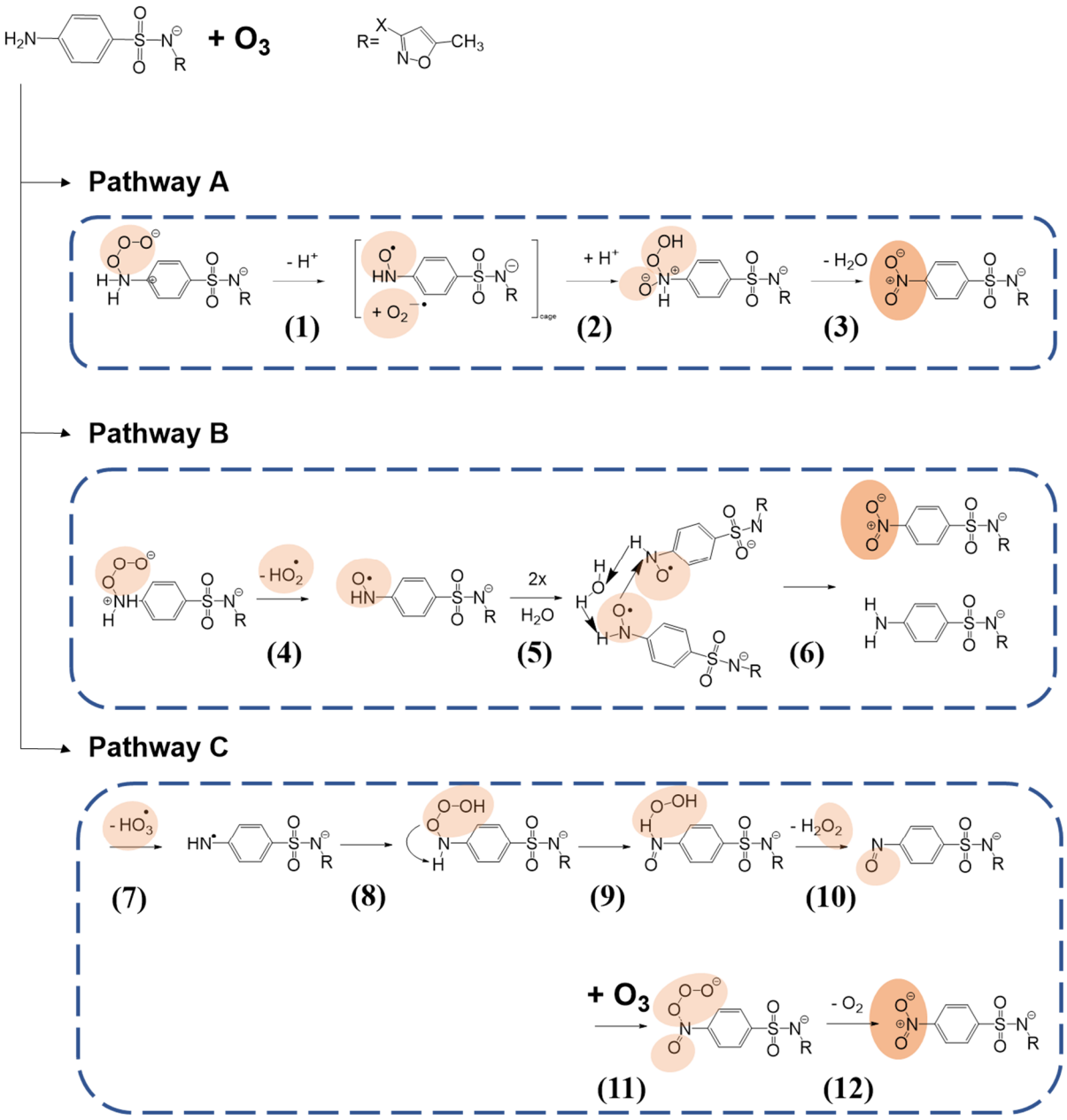

Figure 6. Three proposed formation pathway for the formation of 4-nitro-

427 sulfamethoxazole (Extracted Willach et al. (2017) and Yu et al. (2017)). Orange circles
428 highlight the presence of ^{18}O.

429 ^{18}O labels in the proposed hydroxylated structures OP282b/c and OP268 indicate that
430 hydroxylation predominately follows an oxygen transfer (addition) reaction as
431 described by Tekle-Röttering et al. (2016) for aniline. In the case of OP268, a single
432 hydroxylated OP, it was not possible to separate the two isomers described by Willach
433 et al. (2017). In their study, they confirmed that one of these isomers was
434 sulfamethoxazole hydroxylamine (OP268b), which can imply that the other detected
435 isomer of OP268 (OP268a) could be formed by the reaction of ozone with the aromatic
436 ring (SI, Figure S 8, pathway D). They proposed a formation pathway starting with an
437 H-abstraction from the anilinic nitrogen leading to the formation of an aminyl radical
438 (Yu et al., 2017). This aminyl radical would then react with oxygen to form a peroxyl
439 radical, which would imply the reaction of two peroxyl radicals, and their decay via the
440 Russell mechanism to finally form the hydroxylamine (SI, Figure S 8, pathway E). In
441 this formation pathway the transferred oxygen atom has its origin in the reaction of the
442 aminyl radical with an oxygen molecule, which is contradicted by the observed shift in
443 the isotope pattern of the formed OP268 (see Figure 5). Therefore, the formation
444 pathway for the detected OP268a is better described by the transfer of an oxygen atom
445 from the ozone molecule (Figure 7), although the precise location of the labeled oxygen
446 could not be distinguished between the aromatic ring or the nitrogen moiety.

447 Gómez-Ramos et al. (2011) previously proposed the structure of OP282 b/c in Figure
448 4 based on HRMS measurements and the fragmentation pattern observed, which
449 agrees with the results obtained in our work. For the formation of OP282 b/c (Figure 7)
450 two oxidation equivalents were considered to propose a possible formation pathway.
451 Here the initiation of the reaction could also start as the suggested pathway C for the
452 formation of NIT (Figure 6, reaction (7)-(10)), with the difference that the reaction at
453 the nitrogen would terminate after formation of the nitroso-group and the second ozone
454 attack would follow an oxygen transfer at the aromatic ring (pathway D) (SI, Figure S
455 9). The reason for suggesting the aromatic ring as one of the reaction sites for ozone
456 is due to the observed retention times for OP282 b/c (OP282b R_t: 6.7 min, OP282c R_t:
457 7.1 min) and their fragmentation patterns (SI, Figure S 11, Figure S 12). Furthermore,
458 these two isomers are clearly not related to NIT, due to their significantly shorter
459 retention times (NIT R_t: 17.2 min).

460 According to the mass spectrometric fragmentation pattern observed for OP284 (SI,
461 Figure S 13), this compound is formed by the addition of two oxygen atoms to the
462 aniline ring structure (Figure 7). Its proposed structure presents hydroxylation at the
463 nitrogen and the aromatic ring, but as mentioned above, only one of the two oxygens
464 is labeled. Based on this observation, we propose that the labeled oxygen comes from
465 the direct addition of ozone to the aromatic ring of the aniline (pathway D), while the
466 second oxygen originates from an electron transfer reaction that occurs at the nitrogen
467 moiety (SI, Figure S 8, pathway E). As mentioned in the previous section, the
468 production of this OP was limited and some uncertainty remains regarding the
469 possibility of both oxygen atoms having their origin in direct oxygen transfers from the
470 ozone molecule.

471 The suggested reactions are summarized as a proposed pathway for the
472 transformation of SMX in Figure 7. Some of the intermediates expected after the first
473 ozone attack (nitroso sulfamethoxazole and sulfamethoxazole hydroxylamine) were
474 not detected in this study, but the SMX hydroxylamine was reported previously (Willach
475 et al., 2017). Nonetheless, the formation pathway proposed in Figure 7 agrees with
476 those previously established by Von Sonntag and Von Gunten (2012); Willach et al.
477 (2017).

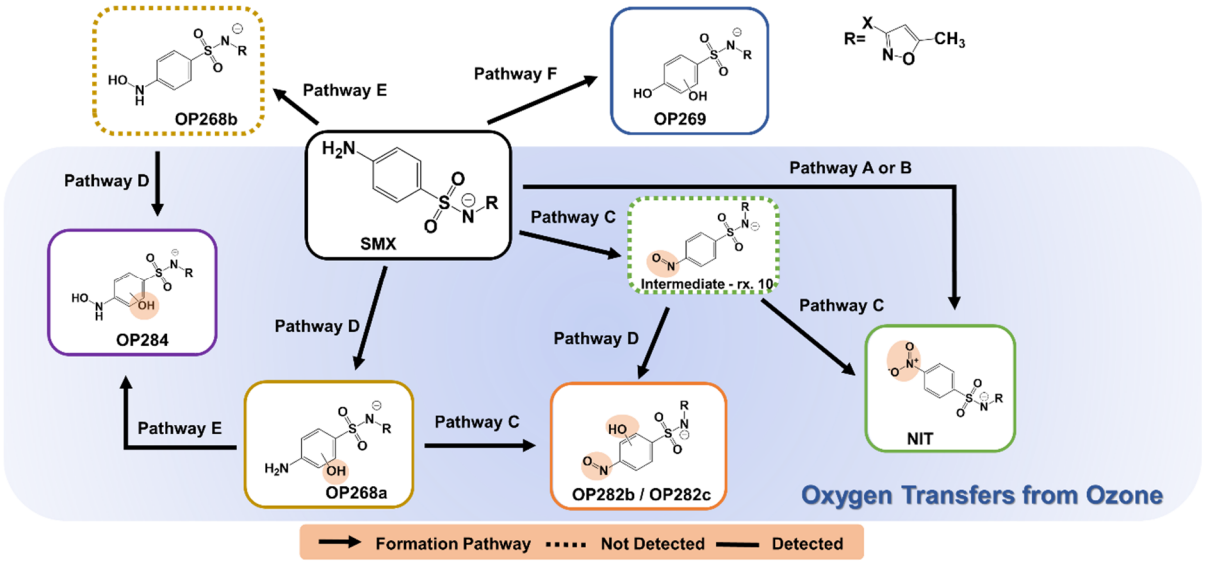

478

479 Figure 7. Overview of the formation pathways involved in the formation of six of the
480 OPs of SMX. Detailed individual pathways are illustrated in Figures 7, S8, S9 and S10.
481 Orange circles highlight the presence of ^{18}O.

482 For the formation of OP269, we can exclude a two-step reaction involving the
483 hydroxylation of the aromatic ring by an oxygen transfer reaction, due to the lack of

484 ^{18}O-labeling observed in the formed OP (see Figure 5). Furthermore, our results agree
485 with the formation pathway proposed by Willach et al. (2017) for OP269, who
486 hypothesized that the formation pathway is initiated by an ozone reaction in the
487 aromatic ring, resulting in an electron transfer reaction (SI, Figure S 10, pathway F).
488 The following reactions result in the cleavage of the anilinic nitrogen from the aromatic
489 ring and its replacement by a quinone group (Willach et al., 2017).

490 Only one form of OP226 could be detected in the different ozonation experiments,
491 unlike the two isomers reported by (Willach et al., 2017). Therefore, it can be concluded
492 that the OP226 detected is not being produced by the reaction of SMX with a hydroxyl
493 radical because of the presence of a radical scavenger. Furthermore, it can be stated
494 with some certainty that the formation pathway involves the transfer of one oxygen
495 atom from ozone.

496 Overall, the successful labeling of six of the seven detected SMX OPs confirmed the
497 applicability of the new method to track the formation of ozonation products from
498 compounds with aniline moieties. Furthermore, the $^{18}O/^{16}O$ ratio provided by the
499 labeling of NOV was paramount to understand the origin of the transferred oxygen
500 atoms and thereby supported the differentiation of previously proposed transformation
501 pathways from oxygen transfer or electron transfer reactions.

502 4. Conclusions

503 This study presented a novel labeling technique with the aim of generating transferable
504 knowledge of ozone reactions, as well as, elucidating formation pathways of OPs. The
505 major conclusions are:

506 • The formation of labeled venlafaxine N-oxide (+2 Da) confirmed the transfer of one
507 ^{18}O atom to the tertiary amine of the model compound. The ratio of $^{18}O/^{16}O$ in the
508 formed venlafaxine N-oxide correlated with determined gas ratios in previous tracer
509 tests with N_2 and O_2 at the same operational settings. Therefore, venlafaxine N-
510 oxide can be used as an indicator of ^{18}O purity in the system. The measured $^{18}O/^{16}O$
511 ratios obtained from NOV formation can be used to confirm the origin of the
512 transferred oxygens in newly formed OPs.
513 • The results corroborate that the labeling technique can be used to study the reaction
514 mechanism of ozone, when a transfer of oxygen is involved. Consequently, we

515 present the use of $^{18}O_3$ as a suitable tool to investigate the reaction of ozone with
516 organic chemicals in a wide range of scenarios.
517 • Besides the observed suitability for the elucidation of formation mechanisms and
518 pathways, the integration of this new labeling method will enable the detection of
519 OPs from chemicals with multiple reactive sites and in complex water matrices. In a
520 parallel study this approach has already been applied to identify OBPs formed when
521 effluent organic matter from secondary effluent is ozonated.
522 • An additional potential application of this labeling method is the tracking of OPs and
523 their characteristic newly formed functional groups in biological post-treatment to
524 better understand their stability and persistence in the environment. The presence
525 of the labeled functional group can be used to assess the generation of recalcitrant
526 and potentially toxic OPs in complex water scenarios.

527 5. Declaration of Competing Interest

528 The authors declare no known competing financial interest or personal relationship that
529 could have influence on the work reported in this paper.

530 6. Acknowledgments

531 This study was funded by the Deutsche Forschungsgemeinschaft (DFG-German
532 Research Foundation) under the Project Numbers 428639365 (GZ: HU 2699/1-1 and
533 RE 1290/8-1). We would like to thank Danika Ahoor (TUM) for her contributions in
534 solving the gas humidity problems, Dr. Ignacio Sottorff (TUM) for his consistent support
535 and understanding, and Elaine Jennings (UFZ) for feedback and discussion.

536 7. References

537 Bader, H. 1982. Determination of Ozone In Water By The Indigo Method: A Submitted
538 Standard Method. Ozone: Science & Engineering 4(4), 169-176.
539 https://doi.org/10.1080/01919518208550955.
540 Betsholtz, A., Juárez, R., Svahn, O., Davidsson, Å., Cimbritz, M. and Falås, P. 2022.
541 Ozonation of 14C-labeled micropollutants – mineralization of labeled moieties and
542 adsorption of transformation products to activated carbon. Water Research 221,
543 118738. https://doi.org/10.1016/j.watres.2022.118738.
544 Borowska, E., Bourgin, M., Hollender, J., Kienle, C., McArdell, C.S. and von Gunten, U. 2016.
545 Oxidation of cetirizine, fexofenadine and hydrochlorothiazide during ozonation: Kinetics
546 and formation of transformation products. Water Research 94, 350-362.
547 https://doi.org/10.1016/j.watres.2016.02.020.

548 Bourgin, M., Beck, B., Boehler, M., Borowska, E., Fleiner, J., Salhi, E., Teichler, R., von
549 Gunten, U., Siegrist, H. and McArdell, C.S. 2018. Evaluation of a full-scale wastewater
550 treatment plant upgraded with ozonation and biological post-treatments: Abatement of
551 micropollutants, formation of transformation products and oxidation by-products. Water
552 Research 129, 486-498. https://doi.org/10.1016/j.watres.2017.10.036.
553 Brunner, A.M., Vughs, D., Siegers, W., Bertelkamp, C., Hofman-Caris, R., Kolkman, A. and ter
554 Laak, T. 2019. Monitoring transformation product formation in the drinking water
555 treatments rapid sand filtration and ozonation. Chemosphere 214, 801-811.
556 https://doi.org/10.1016/j.chemosphere.2018.09.140.
557 Dodd, M.C. and Huang, C.-H. 2004. Transformation of the Antibacterial Agent
558 Sulfamethoxazole in Reactions with Chlorine: Kinetics, Mechanisms, and Pathways.
559 Environmental Science & Technology 38(21), 5607-5615.
560 https://doi.org/10.1021/es035225z.
561 Dodd, M.C., Rentsch, D., Singer, H.P., Kohler, H.-P.E. and von Gunten, U. 2010.
562 Transformation of β-Lactam Antibacterial Agents during Aqueous Ozonation: Reaction
563 Pathways and Quantitative Bioassay of Biologically-Active Oxidation Products.
564 Environmental Science & Technology 44(15), 5940-5948.
565 https://doi.org/10.1021/es101061w.
566 Eggen, R.I.L., Hollender, J., Joss, A., Schärer, M. and Stamm, C. 2014. Reducing the
567 Discharge of Micropollutants in the Aquatic Environment: The Benefits of Upgrading
568 Wastewater Treatment Plants. Environmental Science & Technology 48(14), 7683-
569 7689. https://doi.org/10.1021/es500907n.
570 Gao, S., Zhao, Z., Xu, Y., Tian, J., Qi, H., Lin, W. and Cui, F. 2014. Oxidation of
571 sulfamethoxazole (SMX) by chlorine, ozone and permanganate - A comparative study.
572 Journal of Hazardous Materials 274, 258-269.
573 https://doi.org/10.1016/j.jhazmat.2014.04.024.
574 Gómez-Ramos, M.d.M., Mezcua, M., Agüera, A., Fernández-Alba, A.R., Gonzalo, S.,
575 Rodríguez, A. and Rosal, R. 2011. Chemical and toxicological evolution of the
576 antibiotic sulfamethoxazole under ozone treatment in water solution. Journal of
577 Hazardous Materials 192(1), 18-25. https://doi.org/10.1016/j.jhazmat.2011.04.072.
578 Gulde, R., Clerc, B., Rutsch, M., Helbing, J., Salhi, E., McArdell, C.S. and von Gunten, U.
579 2021. Oxidation of 51 micropollutants during drinking water ozonation: Formation of
580 transformation products and their fate during biological post-filtration. Water Research
581 207, 117812. https://doi.org/10.1016/j.watres.2021.117812.
582 Huber, M.M., Göbel, A., Joss, A., Hermann, N., Löffler, D., McArdell, C.S., Ried, A., Siegrist,
583 H., Ternes, T.A. and von Gunten, U. 2005. Oxidation of Pharmaceuticals during
584 Ozonation of Municipal Wastewater Effluents: A Pilot Study. Environmental Science &
585 Technology 39(11), 4290-4299. https://doi.org/10.1021/es048396s.
586 Huber, M.M., Ternes, T.A. and von Gunten, U. 2004. Removal of Estrogenic Activity and
587 Formation of Oxidation Products during Ozonation of 17α-Ethinylestradiol.
588 Environmental Science & Technology 38(19), 5177-5186.
589 https://doi.org/10.1021/es035205x.
590 Hübner, U., von Gunten, U. and Jekel, M. 2015. Evaluation of the persistence of
591 transformation products from ozonation of trace organic compounds–a critical review.
592 Water Research 68, 150-170. https://doi.org/10.1016/j.watres.2014.09.051.
593 Jennings, E., Sierra Olea, M., Michael Kaesler, J., Hübner, U., Reemtsma, T. and Lechtenfeld,
594 O.J. under review. Stable Isotope Labeling for Detection of Ozonation Byproducts in
595 Effluent Organic Matter with FT-ICR-MS. Water Research.
596 Kolkman, A., Martijn, B.J., Vughs, D., Baken, K.A. and van Wezel, A.P. 2015. Tracing
597 Nitrogenous Disinfection Byproducts after Medium Pressure UV Water Treatment by
598 Stable Isotope Labeling and High Resolution Mass Spectrometry. Environmental
599 Science & Technology 49(7), 4458-4465. https://doi.org/10.1021/es506063h.
600 Lee, Y. and Von Gunten, U. 2016. Advances in predicting organic contaminant abatement
601 during ozonation of municipal wastewater effluent: reaction kinetics, transformation
602 products, and changes of biological effects. Environmental Science: Water Research
603 & Technology 2(3), 421-442. https://doi.org/10.1039/C6EW00025H.

604 Lim, S., McArdell, C.S. and von Gunten, U. 2019. Reactions of aliphatic amines with ozone:
605 Kinetics and mechanisms. Water Research 157, 514-528.
606 https://doi.org/10.1016/j.watres.2019.03.089.
607 Lim, S., Shi, J.L., von Gunten, U. and McCurry, D.L. 2022. Ozonation of Organic Compounds
608 in Water and Wastewater: A Critical Review. Water Research, 118053.
609 https://doi.org/10.1016/j.watres.2022.118053.
610 Liu, Z., Craven, C.B., Huang, G., Jiang, P., Wu, D. and Li, X.-F. 2019. Stable Isotopic Labeling
611 and Nontarget Identification of Nanogram/Liter Amino Contaminants in Water.
612 Analytical Chemistry 91(20), 13213-13221.
613 https://doi.org/10.1021/acs.analchem.9b03642.
614 Loos, M., Gerber, C., Corona, F., Hollender, J. and Singer, H. 2015. Accelerated isotope fine
615 structure calculation using pruned transition trees. Analytical Chemistry 87(11), 5738-
616 5744. https://doi.org/10.1021/acs.analchem.5b00941.
617 Loos, R., Carvalho, R., António, D.C., Comero, S., Locoro, G., Tavazzi, S., Paracchini, B.,
618 Ghiani, M., Lettieri, T., Blaha, L., Jarosova, B., Voorspoels, S., Servaes, K., Haglund,
619 P., Fick, J., Lindberg, R.H., Schwesig, D. and Gawlik, B.M. 2013. EU-wide monitoring
620 survey on emerging polar organic contaminants in wastewater treatment plant
621 effluents. Water Research 47(17), 6475-6487.
622 https://doi.org/10.1016/j.watres.2013.08.024.
623 Mairinger, T. and Hann, S. (2020) Metabolic Flux Analysis in Eukaryotic Cells: Methods and
624 Protocols. Nagrath, D. (ed), pp. 1-16, Springer US, New York, NY.
625 https://doi.org/10.1007/978-1-0716-0159-4_1.

626 Margot, J., Kienle, C., Magnet, A., Weil, M., Rossi, L., de Alencastro, L.F., Abegglen, C.,
627 Thonney, D., Chèvre, N., Schärer, M. and Barry, D.A. 2013. Treatment of
628 micropollutants in municipal wastewater: Ozone or powdered activated carbon?
629 Science of the Total Environment 461-462, 480-498.
630 https://doi.org/10.1016/j.scitotenv.2013.05.034.
631 Mawhinney, D.B., Vanderford, B.J. and Snyder, S.A. 2012. Transformation of 1H-
632 Benzotriazole by Ozone in Aqueous Solution. Environmental Science & Technology
633 46(13), 7102-7111. https://doi.org/10.1021/es300338e.
634 Müller, J., Drewes, J.E. and Hübner, U. 2017. Sequential biofiltration–A novel approach for
635 enhanced biological removal of trace organic chemicals from wastewater treatment
636 plant effluent. Water Research 127, 127-138.
637 https://doi.org/10.1016/j.watres.2017.10.009.
638 Müller, J., Drewes, J.E. and Hübner, U. 2019. Investigating synergies in sequential
639 biofiltration-based hybrid systems for the enhanced removal of trace organic chemicals
640 from wastewater treatment plant effluents. Environmental Science: Water Research &
641 Technology 5(8), 1423-1435. https://doi.org/10.1039/C9EW00181F.
642 Real, F.J., Benitez, F.J., Acero, J.L., Sagasti, J.J.P. and Casas, F. 2009. Kinetics of the
643 Chemical Oxidation of the Pharmaceuticals Primidone, Ketoprofen, and Diatrizoate in
644 Ultrapure and Natural Waters. Industrial & Engineering Chemistry Research 48(7),
645 3380-3388. https://doi.org/10.1021/ie801762p.
646 Reemtsma, T., Weiss, S., Mueller, J., Petrovic, M., González, S., Barcelo, D., Ventura, F. and
647 Knepper, T.P. 2006. Polar Pollutants Entry into the Water Cycle by Municipal
648 Wastewater: A European Perspective. Environmental Science & Technology 40(17),
649 5451-5458. https://doi.org/10.1021/es060908a.
650 Spahr, S., Bolotin, J., Schleucher, J., Ehlers, I., von Gunten, U. and Hofstetter, T.B. 2015.
651 Compound-Specific Carbon, Nitrogen, and Hydrogen Isotope Analysis of N-
652 Nitrosodimethylamine in Aqueous Solutions. Analytical Chemistry 87(5), 2916-2924.
653 https://doi.org/10.1021/ac5044169.
654 Spahr, S., von Gunten, U. and Hofstetter, T.B. 2017. Carbon, Hydrogen, and Nitrogen Isotope
655 Fractionation Trends in N-Nitrosodimethylamine Reflect the Formation Pathway during
656 Chloramination of Tertiary Amines. Environmental Science & Technology 51(22),
657 13170-13179. https://doi.org/10.1021/acs.est.7b03919.

Tekle-Röttering, A., von Sonntag, C., Reisz, E., Eyser, C.v., Lutze, H.V., Türk, J., Naumov, S., Schmidt, W. and Schmidt, T.C. 2016. Ozonation of anilines: Kinetics, stoichiometry, product identification and elucidation of pathways. Water Research 98, 147-159. https://doi.org/10.1016/j.watres.2016.04.001.

Tentscher, P.R., Lee, M. and von Gunten, U. 2019. Micropollutant Oxidation Studied by Quantum Chemical Computations: Methodology and Applications to Thermodynamics, Kinetics, and Reaction Mechanisms. Accounts of Chemical Research 52(3), 605-614. https://doi.org/10.1021/acs.accounts.8b00610.

Ternes, T.A., Stüber, J., Herrmann, N., McDowell, D., Ried, A., Kampmann, M. and Teiser, B. 2003. Ozonation: a tool for removal of pharmaceuticals, contrast media and musk fragrances from wastewater? Water Research 37(8), 1976-1982. https://doi.org/10.1016/S0043-1354(02)00570-5.

Valkenborg, D., Mertens, I., Lemière, F., Witters, E. and Burzykowski, T. 2012. The isotopic distribution conundrum. Mass Spectrometry Reviews 31(1), 96-109. https://doi.org/10.1002/mas.20339.

von Gunten, U. 2003. Ozonation of drinking water: Part I. Oxidation kinetics and product formation. Water Research 37(7), 1443-1467. https://doi.org/10.1016/S0043-1354(02)00457-8.

von Gunten, U. 2018. Oxidation Processes in Water Treatment: Are We on Track? Environmental Science & Technology 52(9), 5062-5075. https://doi.org/10.1021/acs.est.8b00586.

Von Sonntag, C. and Von Gunten, U. (2012) Chemistry of ozone in water and wastewater treatment, IWA publishing. https://doi.org/10.2166/9781780400839.

Wert, E.C., Rosario-Ortiz, F.L., Drury, D.D. and Snyder, S.A. 2007. Formation of oxidation byproducts from ozonation of wastewater. Water Research 41(7), 1481-1490. https://doi.org/10.1016/j.watres.2007.01.020.

Willach, S., Lutze, H.V., Eckey, K., Löppenberg, K., Lüling, M., Terhalle, J., Wolbert, J.-B., Jochmann, M.A., Karst, U. and Schmidt, T.C. 2017. Degradation of sulfamethoxazole using ozone and chlorine dioxide - Compound-specific stable isotope analysis, transformation product analysis and mechanistic aspects. Water Research 122, 280-289. https://doi.org/10.1016/j.watres.2017.06.001.

Yu, H., Ge, P., Chen, J., Xie, H. and Luo, Y. 2017. The degradation mechanism of sulfamethoxazole under ozonation: a DFT study. Environmental Science: Processes & Impacts 19(3), 379-387. https://doi.org/10.1039/C6EM00698A.

Zucker, I., Mamane, H., Riani, A., Gozlan, I. and Avisar, D. 2018. Formation and degradation of N-oxide venlafaxine during ozonation and biological post-treatment. Science of the Total Environment 619, 578-586. https://doi.org/10.1016/j.scitotenv.2017.11.133.

non-peer reviewed EarthArXiv preprint – submitted and under review in "Water Research"

Supplementary Information

Isotopically labeled ozone in functional group ozonation: a new approach for elucidating ozonation products formation

Millaray Sierra Olea[a], Simon Kölle[a], Emil Bein[a], Thorsten Reemtsma[b], Oliver J. Lechtenfeld[b], and Uwe Hübner[a]*

[a] Chair of Urban Water Systems Engineering, Technical University of Munich, Am Coulombwall 3, D-85748 Garching, Germany

[b] Department of Analytical Chemistry, Helmholtz Centre for Environmental Research – UFZ, Permoserstrasse 15, 04318 Leipzig, Germany

* Corresponding author: Chair of Urban Water Systems Engineering, Technical University of Munich, Am Coulombwall 3, D-85748 Garching, Germany

E-mail: u.huebner@tum.de (U. Hübner)

Table of Contents

Supplementary Information

Table S 1: List of used chemicals.

Chemicals	Supplier	CAS.No
Indigo Carmine, 80% purity	*Carl Roth GmbH*, EG-No: 212-728-8	
Labeled Oxygen ($^{18}O_2$)	97% purity*, 1 bar, Linde Gas*	
Molecular Sieve / Zeolite	0.3 nm, ~2 mm beads, Supelco,1.05704.1000	1318-02-1
Nitrogen (N_2)	≥ 99,8 %, “Nitrogen 2.8”, 300 bar, *Air Liquide*	
Oxygen ($^{16}O_2$)	≥ 99,95 % “Oxygen 3.5”, 300 bar, *Air Liquide*	
Phosphoric Acid	85 %, *Emsure*, 1.00573.1000	
Primidone	Fluka Analytics	125-33-7
Sulfamethoxazole	Fluka Analytics	723-46-6
4-Nitro Sulfamethoxazole	Toronto Research Chemicals	29699-89-6
tert-Butanol, ≥99.0 %	Carl Roth GmbH	75-65-0
Venlafaxine (VLX Hydrochlorid)	Sigma-Aldrich	99300-78-4
Venlafaxine N-Oxide	Toronto Research Chemicals	1094598-37-4

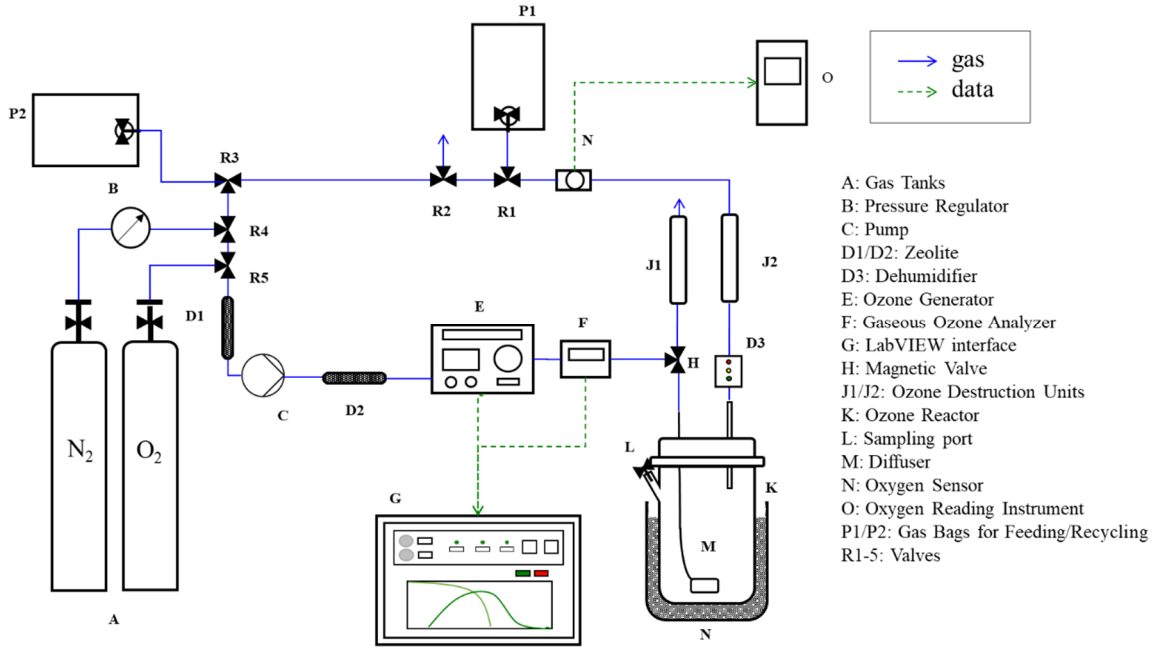

Figure S 1: Design of an ozonation system modified for oxidation with $^{18}O_2$.

Table S 2: List of the equipment, materials and chemicals used for the ozonation setup.

Gas bags (Q)	Bag, Multi-Layer, 3 Liter, Polypropylene Combo Valve with Replaceable Septum, 1 Eyelet, Catalog #: 22951. *Restek*
Hoses	Material: PTFE, 6/4x1. *Serto AG*
Magnetic Valve (H)	Plunger Valve 3/2-way direct acting, for liquid and gaseous media. Type 0355. *Bürkert – Fluid Control Systems*
Oxygen Reading Instrument (P)	Fibox 4 Fiber Optic Oxygen Transmitter. *PreSens Precision Sensing*
Oxygen Sensor (O)	Single-Use Flow-Through Cell O_2 FTC-SU-PSt3. *Presens Precision Sensing*
Ozone Analyzer (F)	Ozone Analyzer BMT 964, in-gas (range: 300 g/Nm³) off-gas (range: 50 g/Nm³). *BMT Messtechnik GmbH*
Ozone Destruction Units (J)	CAT-RS. *BMT Messtechnik GmbH*
Ozone Generator (E)	BMT 803 BT (Bench Top), air cooled. *BMT Messtechnik GmbH*
Ozone Reactor (K)	Duran Glass Bottle (500 mL) with integrated outlet for the sampling port (L)
Pump (C)	MP-F05, Performance: 320 Nl/H, *M&C TechGroup Germany GmbH*
Sampling syringes and needles	Long-life Instrument Syringe, 1 mL, 2.5 mL and 100 µL. *SGE*
Valve R1-3	3-way T ball valve with locking handle. *Osmobil*
Valve R4	ball valve, QH-QS-6-1/8 with plug connection. *Festo*

Table S 3: Batch experiment sample composition.

	Compound Concentrations [µmol L^{-1}]				
Sample	VLX	SMX	PRI	t-BuOH	Buffer
VLX_ #	20	0	3	10000	50000
SMX_#	10	50	3	150000	50000

Table S 4: Targeted molar ratios for the ozonation of compounds.

VLX		**VLX/SMX**	
Ozone Conc. (µmol L^{-1})	**Molar Ratio VLX : O_3**	**Ozone Conc. (µmol L^{-1})**	**Molar Ratio VLX/SMX : O_3**
0	1:0	0	1:0
10	1:0.5	50	1:1
20	1:1	100	1:2
30	1:1.5	150	1:3
40	1:2	200	1:4
60	1:2.5	250	1:5
80	1:3	300	1:6
100	1:5		

Table S 5: List of compounds measured with the MRM method.

Expected RT	Compound Name	IS Name	Q1 Mass	Q3 Mass
MRM positive mode				
4.03	Primidone	Primidone-d5	219.10	162.10
4.03	Primidone	Primidone-d5	219.10	119.00
4.65	Venlafaxine	Venlafaxine-d6	278.20	215.20
4.65	Venlafaxine	Venlafaxine-d6	278.20	58.00
4.91	Venlafaxine N-oxid	Venlafaxine-d6	294.10	178.00
4.91	Venlafaxine N-oxid	Venlafaxine-d6	294.10	120.90
4.91	Venlafaxine N-oxid	Venlafaxine-d6	294.10	163.00
4.91	Venlafaxine N-oxid ^{18}O	Venlafaxine-d6	296.10	178.00
4.91	Venlafaxine N-oxid ^{18}O	Venlafaxine-d6	296.10	120.90
4.91	Venlafaxine N-oxid ^{18}O	Venlafaxine-d6	296.10	165.00
4.75	Sulfamethoxazole	Sulfamethoxazole-d4	254.00	156.00
4.75	Sulfamethoxazole	Sulfamethoxazole-d4	254.00	108.00
MRM negative mode				
5.71	4-Nitro Sulfamethoxazole	Cardersartan_d4	282.00	185.90

5.71	4-Nitro Sulfamethoxazole	Cardersartan_d4	282.00	137.90
5.71	4-Nitro Sulfamethoxazole	Cardersartan_d4	284.00	187.90
5.71	4-Nitro Sulfamethoxazole	Cardersartan_d4	284.00	139.90
5.71	4-Nitro Sulfamethoxazole	Cardersartan_d4	286.00	189.90
5.71	4-Nitro Sulfamethoxazole	Cardersartan_d4	286.00	141.90

87

88 Table S 6: Gradient Method.

Time [m]	Composition	
	Mobile Phase-A [%] (Water + 0.1%FA)	Mobile Phase-B [%] (ACN + 0.1%FA)
0.0	100	0
3.5	85	15
7.0	81	19
10.0	75	25
13.0	65	35
15.0	65	35
16.0	0	100
19.0	0	100
19.5	100	0
22.0	100	0

89

90 Table S 7: Mass ranges used in MS^1 and MS^2 experiments.

Scan Type	Mass range [Da]	
	Start	Stop
Enhanced MS Scan (EMS)	224.000	232.000
	280.000	290.000
	266.000	272.000
Enhanced Product Ion Scan (EPI)	90.000	300.000

91

92 Table S 8: Isotopologue peaks ranges of MS^1 scans, focusing on their centroid mass
93 (Da), peak start (Da) and peak end (Da).

	m/z	Centroid mass (Da)	Peak start (da)	Peak End (Da)
282a Rt: 17.2 min				
282				
Ave	282.10	282.10	281.88	282.32
std	0.1829758	0.1810161	0.2567650	0.1803999
min	282.000	281.880	281.640	282.000
max	282.72	282.72	282.88	282.84
284				
Ave	284.164557	284.1540456	284.0020253	284.3043038
std	0.178544023	0.175486081	0.21563201	0.182518829
min	284.04	283.92	283.68	284.04
max	284.88	284.88	284.88	285.24

286				
Ave	286.148	286.1375133	286.0093333	286.3
std	0.160049992	0.160239961	0.270443258	0.198595065
min	286.08	286.02	285.72	286.2
max	286.92	286.92	286.96	287.28
282b Rt: 6.7 min				
282				
Ave	282.1034483	282.1076506	281.9351724	282.2524138
std	0.216942323	0.232476324	0.250001665	0.211426276
min	282	281.88	281.76	282
max	282.96	283.2	282.96	283.2
284				
Ave	284.13	284.1218547	283.99875	284.240625
std	0.076485293	0.076262734	0.085430893	0.084997702
min	284.04	283.92	283.8	284.04
max	284.4	284.4	284.28	284.4
286				
Ave	286.1298113	286.1194094	285.9758491	286.2362264
std	0.067697735	0.056370554	0.073854369	0.082695769
min	286.08	286.05	285.84	286.08
max	286.32	286.32	286.2	286.32
282c Rt: 7.1 min				
282				
Ave	282.09	282.09	281.96	282.22
std	0.179452	0.178004	0.210577	0.177419
min	282.000	281.960	281.640	282.120
max	282.960	282.960	282.960	283.080
284				
Ave	284.1381818	284.1272515	284.0254545	284.2254545
std	0.062350648	0.072211432	0.082281516	0.089072354
min	284.04	283.92	283.8	284.04
max	284.28	284.28	284.16	284.4
286				
Ave	286.1217391	286.1004348	285.9634783	286.226087
std	0.075966364	0.086701801	0.18231861	0.086363193
min	286.08	285.96	285.2	286.08
max	286.32	286.32	286.2	286.44
284 Rt: 6.5 min				
284				
Ave	284.1307317	284.130439	283.9912195	284.2507317

std	0.07853507	0.076173678	0.092451573	0.069013616
min	284.040	284.040	283.800	284.160
max	284.400	284.400	284.280	284.400
286				
Ave	286.1509091	286.1314545	286.0309091	286.2381818
std	0.078097206	0.096214121	0.093366779	0.075776967
min	286.08	285.96	285.84	286.08
max	286.32	286.32	286.2	286.32
268 Rt: 9.8 min				
268				
Ave	268.1132039	268.0991117	267.9401942	268.2518447
std	0.138200738	0.13666597	0.164346193	0.146861982
min	267.96	267.84	267.72	267.96
max	268.92	268.92	268.92	269.04
270				
Ave	270.1730435	270.169642	270.0052174	270.326087
std	0.18331334	0.183825488	0.22233679	0.183865242
min	270	270	269.76	270.12
max	270.96	270.96	270.96	271.32
269 Rt: 10.1				
269				
Ave	269.1361932	269.1201903	268.9670455	269.2504545
std	0.129113002	0.142658273	0.141855873	0.22567026
min	269.04	268.04	268.8	268.28
max	269.92	269.64	269.64	269.76
270				
Ave	270.1169231	270.1076	270.0292308	270.2092308
std	0.108655037	0.100389336	0.092525384	0.091016612
min	270	270	269.88	270.12
max	270.48	270.48	270.36	270.48
271				
Ave	271.1142857	271.0919048	271	271.16
std	0.091785019	0.065291949	0.06761234	0.06761234
min	270.96	270.96	270.84	271.08
max	271.44	271.2	271.08	271.32
226 Rt: 9.8 min				
226				
Ave	226.1014286	226.0822321	225.8657143	226.2428571
std	0.091014688	0.087382856	0.117212523	0.091918331
min	226.08	226.0036	225.72	226.08

max	226.56	226.5	226.32	226.56
228				
Ave	228.1285714	228.0857143	228	228.1457143
std	0.084418781	0.095447389	0.07855844	0.080862695
min	228	227.88	227.88	228
max	228.24	228.24	228.12	228.36

Table S 9: Ranges used for the area integration of the detected SMX OPs.

		Mass Range [Da]	
Name	Expected RT (min)	Start	Stop
TP284_1	6.5	283.8	284.4
TP284_2		285.8	286.4
TP282b_1	6.7	281.7	283.2
TP282b_2		283.8	284.4
TP282b_3		285.8	286.4
TP282c_1	7.1	281.6	283.1
TP282c_2		283.8	284.4
TP282c_3		285.2	286.5
TP226_1	9.8	225.7	226.6
TP226_2		227.8	228.4
TP268_1	9.8	267.7	269.1
TP268_2		296.7	271.4
TP269_1	10.1	268.8	269.8
TP269_2		269.9	270.5
TP269_3		270.9	271.4
TP282a_1	17.2	281.6	282.9
TP282a_2		283.6	285.3
TP282a_3		285.7	287.3

Text S 1: Expected isotopic pattern of SMX + 2O using enviPat platform.

The chemical formula of SMX + 2O isotopologues with relative abundances above the threshold 0.01 were considered and their exact mass was calculated by replacing the natural abundance of ^{16}O (99.757 %), and ^{18}O (0.205 %) (Coursey et al., 2015) and using the calculated ratio of $^{16}O/^{18}O$ as indicated by the mass shift in NOV. The isotope peaks that are relevant for SMX + 2O mass shift are: *m/z* 282 ($^{16}O_2$), *m/z* 284 ($^{16}O_1$ - $^{18}O_1$) and *m/z* 286 ($^{18}O_2$) because of the expected shift in abundance occurs when the direct reaction of ozone with the molecule is successful. According to the results of this exercise, *m/z* 282 $[M-H]^-$ had a 100% of the relative abundance explained by the chemical formula $^{12}C_{10}{}^{1}H_8{}^{14}N_3{}^{16}O_5{}^{32}S$. Meanwhile, *m/z* 284 $[M-H]^-$ is a sum of six isotopologues with the isotope replacements of: ^{34}S (4.474 %), ^{13}C - ^{15}N (0.118 %), ^{13}C - ^{33}S (0.085 %), ^{18}O (1.027 %), $^{13}C_2$ (0.526 %) and ^{13}C - ^{17}O (0.020 %). Finally, *m/z* 286 $[M-H]^-$ is a sum of three isotopologues with the isotope replacements of: ^{36}S (0.010 %), ^{18}O - ^{34}S (0.045 %) and $^{13}C_2$ - ^{34}S (0.023 %). From these results we can conclude that only ± 1.027 % of the 6.25 % relative abundance of *m/z* 284 can be justified by the existence of one ^{18}O, meanwhile, ± 0.045 % of the relative abundance of 0.080 % of *m/z* 286 can be expected to correspond to the presence of ^{18}O - ^{34}S in the molecule.

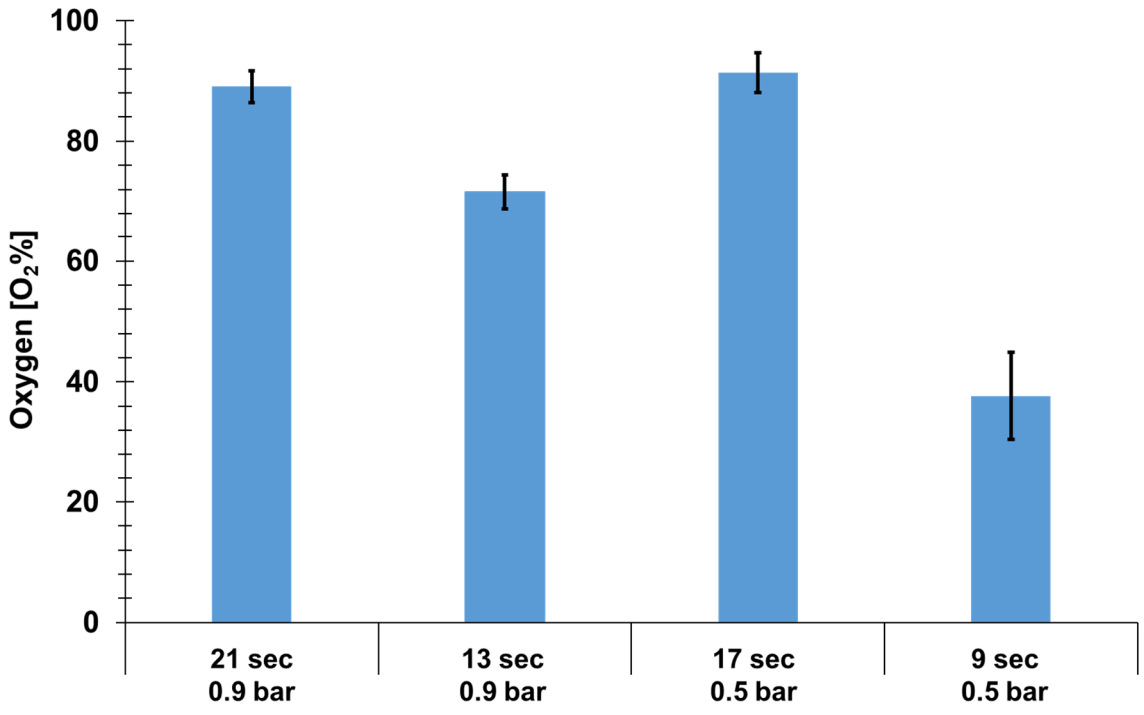

Figure S 2: Impact of gas pressure of the ozone generator on the expected purity of ^{18}O in the system.

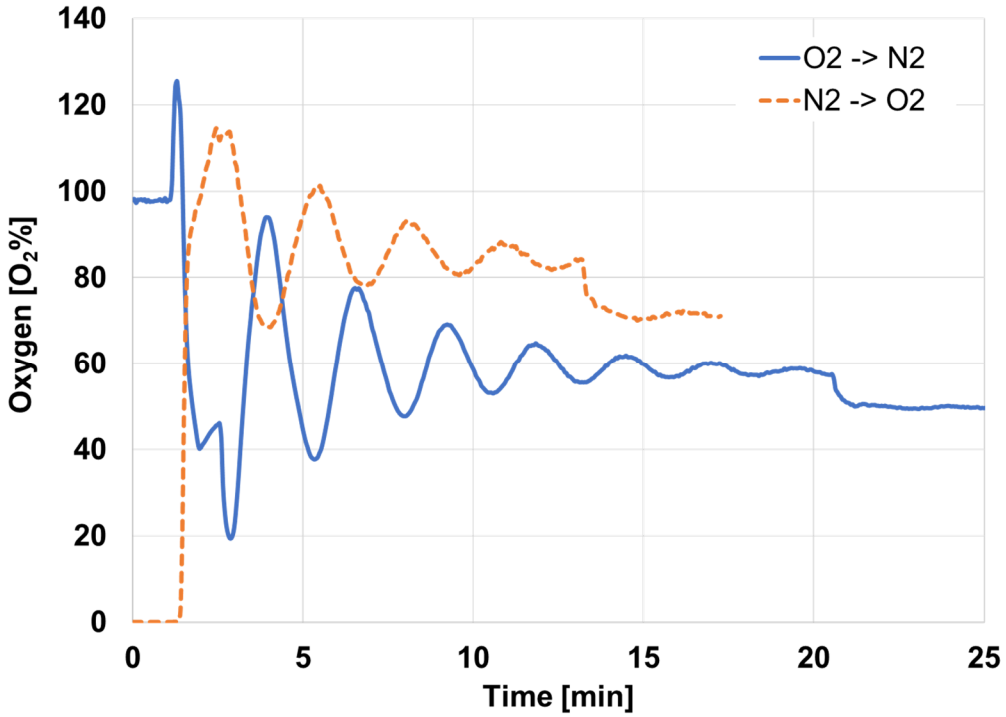

Figure S 3: Impact in the simulated gas purity depending on the gas being exchanged.

Text S 2: Correlation of the pressure with the oxygen measured by the in-line *PreSens* oxygen sensors (A. Schmid, personal communication May 25th, 2022).

$$\%\ O_2(cor.) = \%\ O_2(meas.) \cdot \frac{p_{atm}}{p_{act}}$$

p_{atm}	Atmospheric pressure during calibration
p_{act}	Atmospheric pressure during measurement
$\%\ O_2(cor.)$	$\%\ O_2(cor.)$ corrected
$\%\ O_2(meas.)$	$\%\ O_2(meas.)$ measured

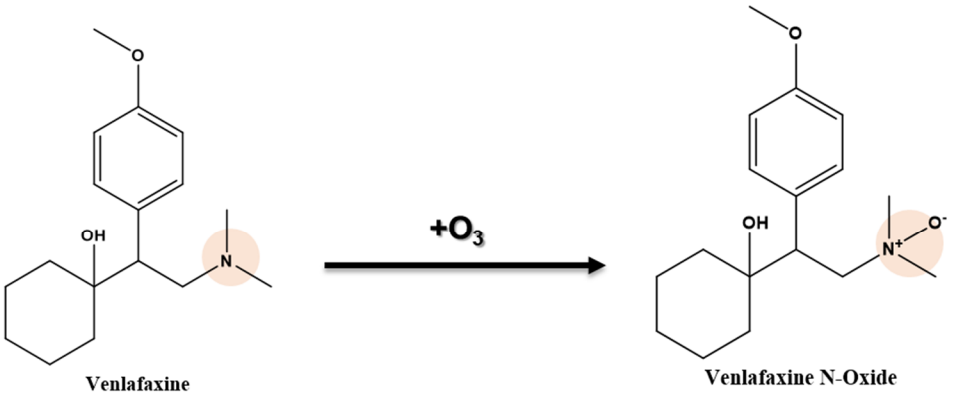

Venlafaxine
Chemical Formula: $C_{17}H_{27}NO_2$
Molecular Weight: 277,41

Venlafaxine N-Oxide
Chemical Formula: $C_{17}H_{27}NO_3$
Molecular Weight: 293,41

Figure S 4: The reaction of VLX with O_3 results in the transfer of one oxygen atom to the nitrogen in the tertiary amine moiety. From this reaction it has been reported a formation of >70% of NOV (Zucker et al., 2018).

Text S 3: Isotope pattern determination for NOV using enviPat platform.

According to the results of this exercise, *m/z* 294 had a 100 % of the relative abundance explained by the chemical formula $^{12}C_{17}{}^{1}H_{28}{}^{14}N_{1}{}^{16}O_3$. Meanwhile, *m/z* 296 is a sum of five isotopologues with the isotope replacements of: ^{13}C - ^{15}N (0.067 %), ^{18}O (0.616 %), $^{13}C_2$ (1.591 %), ^{13}C - ^{17}O (0.021 %) and ^{13}C - ^{2}H (0.059 %). Therefore, only ± 0.616 % of the 3 % measured value can be justified by the existence of ^{18}O in the molecule, and any change in the isotopic pattern of the molecule would be explained by the reaction of VLX with $^{18}O_3$ and the attachment of one 18-oxygen atom to the nitrogen group of the compound.

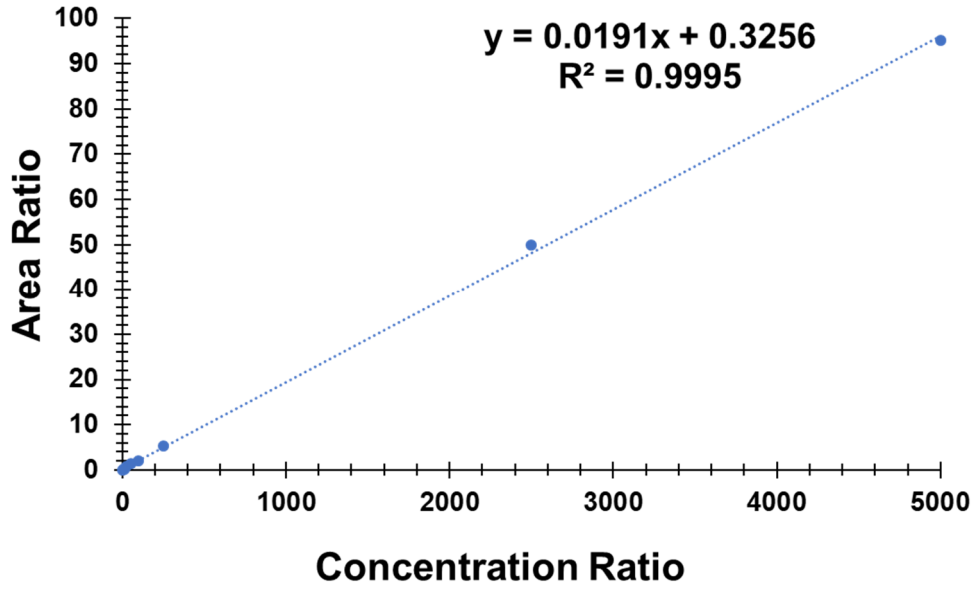

143

144 Figure S 5: 4-nitrosulfamethoxazole calibration curve (ng L^{-1}).

145

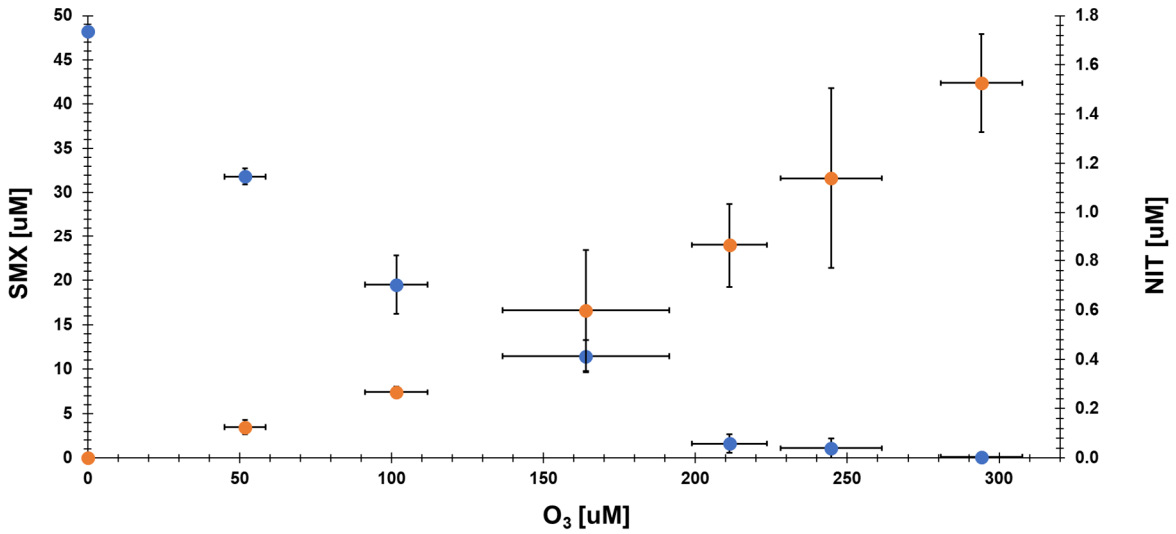

146

147 Figure S 6: Yield of 4-nitrosulfamethoxazole (NIT). Three independent ozonation
148 experiments were performed using different $^{18}O/^{16}O$ ratios for the production of ozone.
149 The targeted SMX : O_3 dose (see SI, **Error! Reference source not found.**) was the
150 same in all experiments. Error bars indicate the standard deviation.

151

152

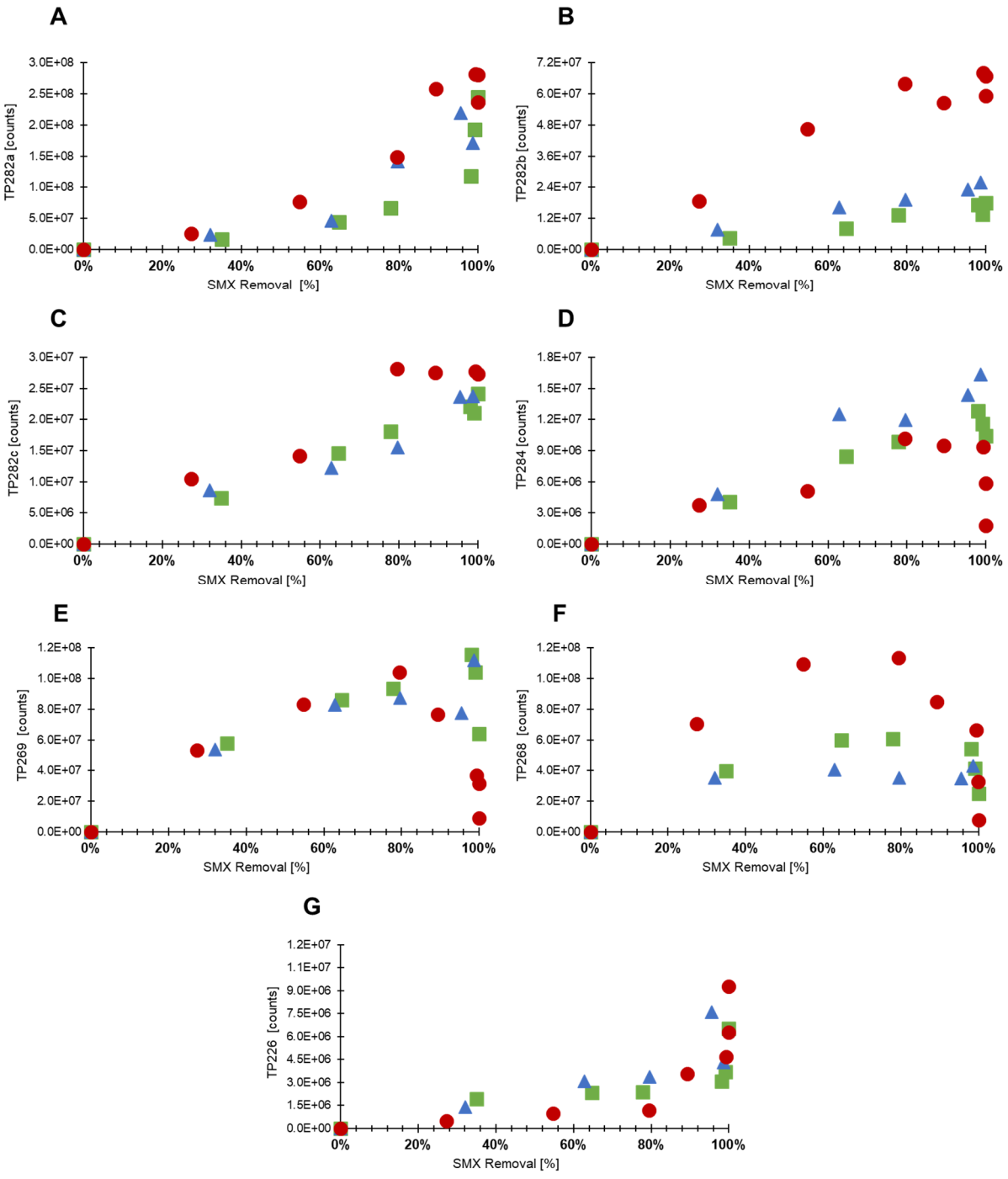

Figure S 7: Removal of SMX and formation of the seven OPs obtained from the ozonation experiments. These OPs are: (**A**) OP282a also identified as 4-nitro sulfamethoxazole (NIT), (**B**) OP282b, (**C**) OP282c, (**D**) OP284, (**E**) OP268, (**F**) OP269, and (**G**) OP226. The number is their m/z when produced by $^{16}O_3$.

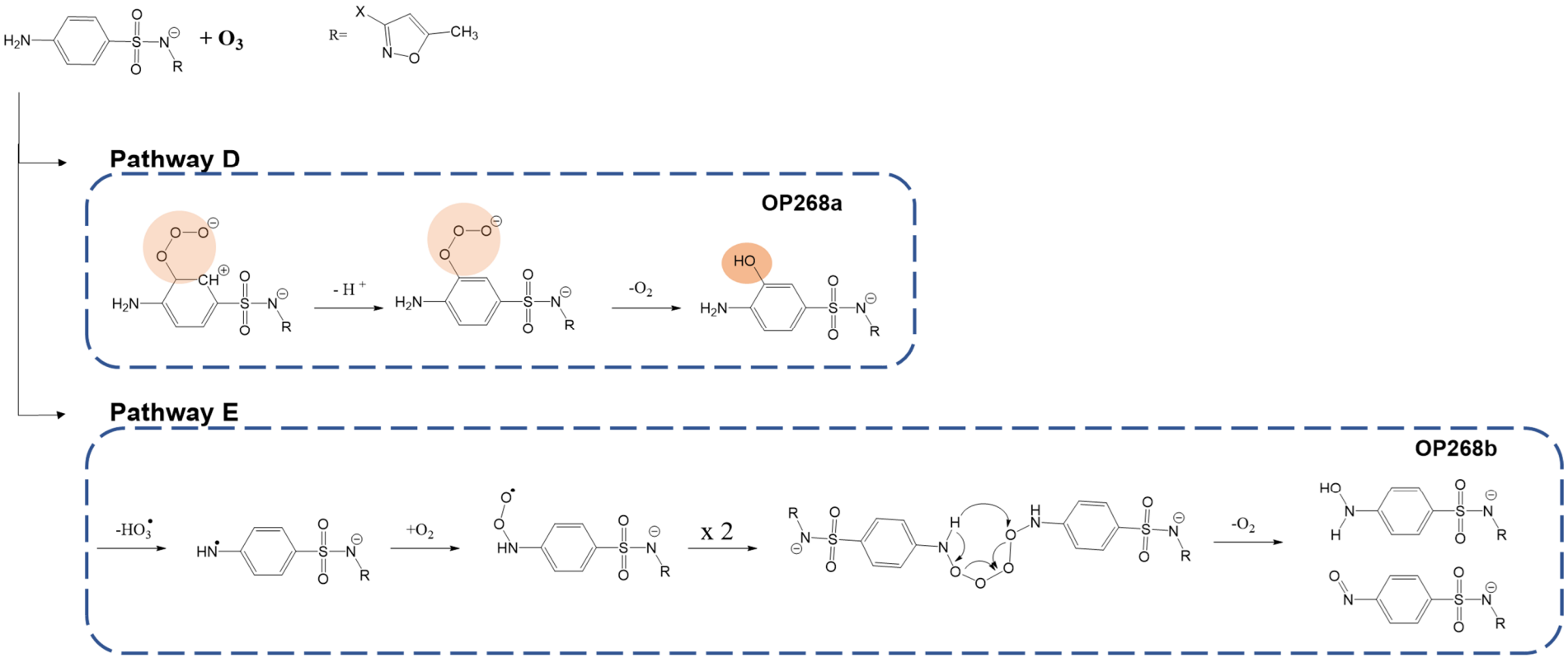

Figure S 8: Proposed reaction mechanism for the formation of the two isomers of OP268 in the reaction with ozone (pathway D and E). The detected OP268a could be formed by an oxygen addition at the aromatic ring (Orange circle highlights the presence of oxygen-18). Meanwhile the undetected OP268b, can be explained by the reaction with ozone and the subsequent formation of sulfamethoxazole hydroxylamine and 4 – nitroso sulfamethoxazole (Extracted Willach et al. (2017)).

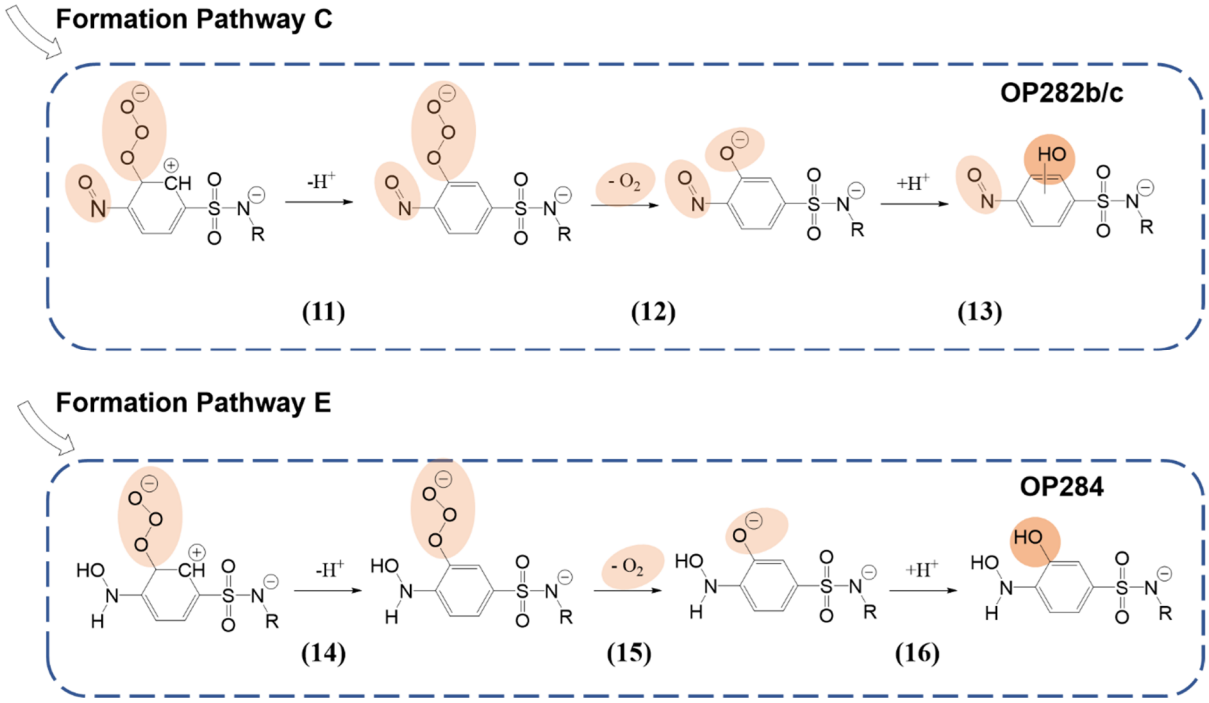

Figure S 9: Proposed reaction mechanism for the formation of OP282 b/c and OP284 in the reaction with ozone. Orange circle highlights the presence of oxygen-18.

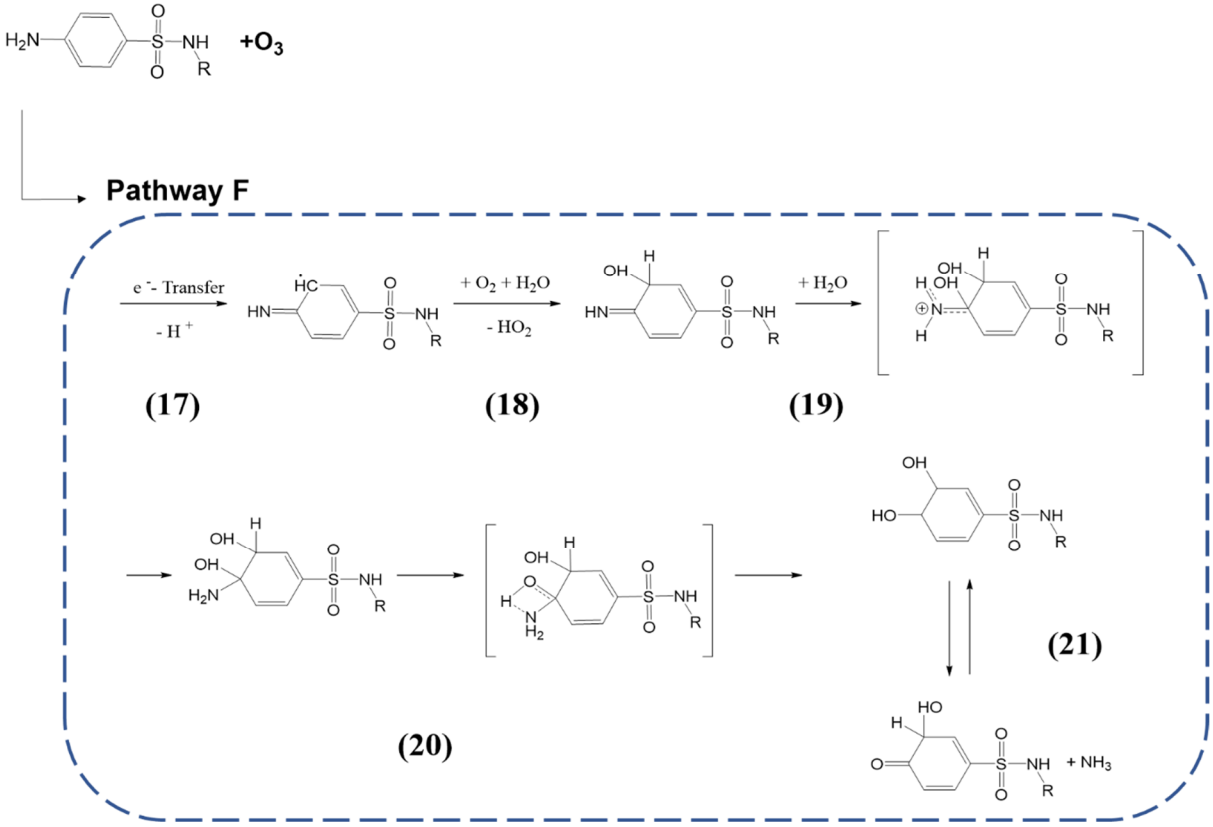

Figure S 10: Proposed reaction mechanism for the formation of OP269 in the reaction with ozone (Extracted from Willach et al. (2017)).

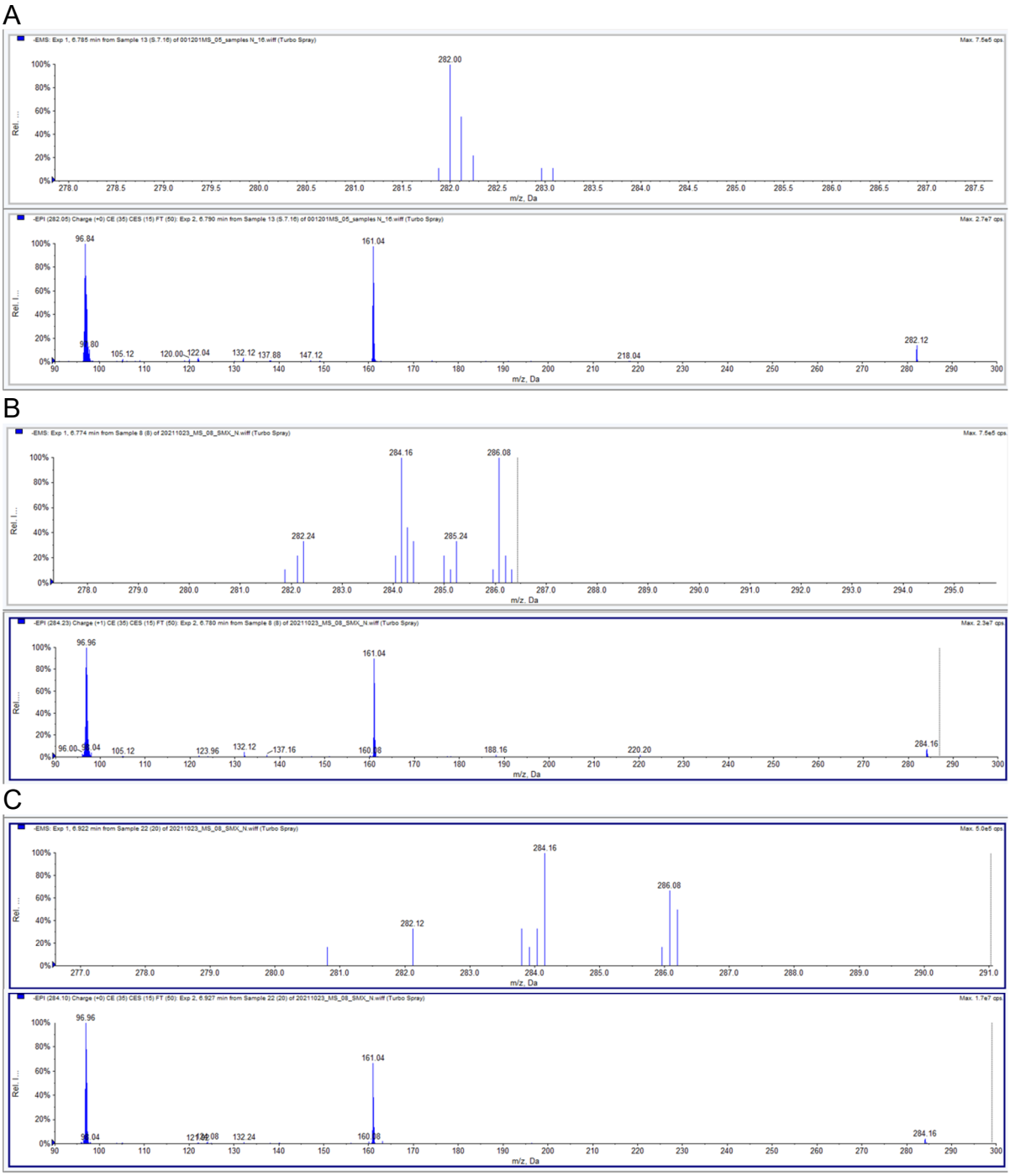

Figure S 11: Fragmentation pattern of OP282b, Rt: 6.7 min. A) ozone produced with technical oxygen ($^{16}O_2$), B) ozone produced with 55% $^{18}O_2$, C) ozone produced with 74% $^{18}O_2$

A

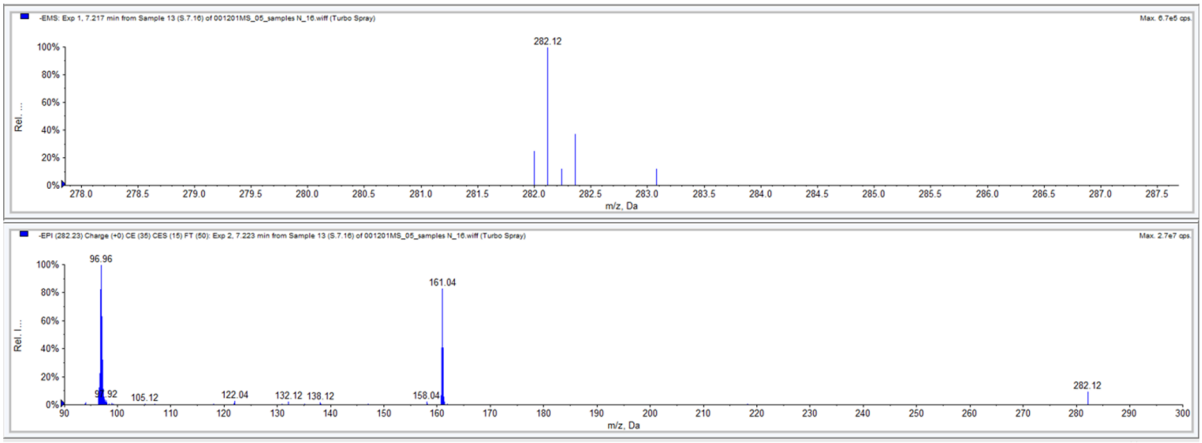

B

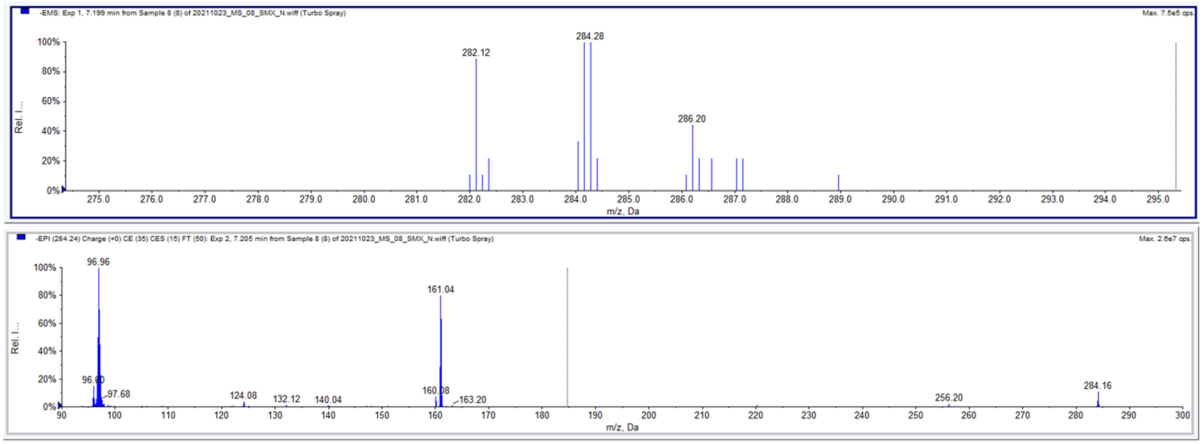

C

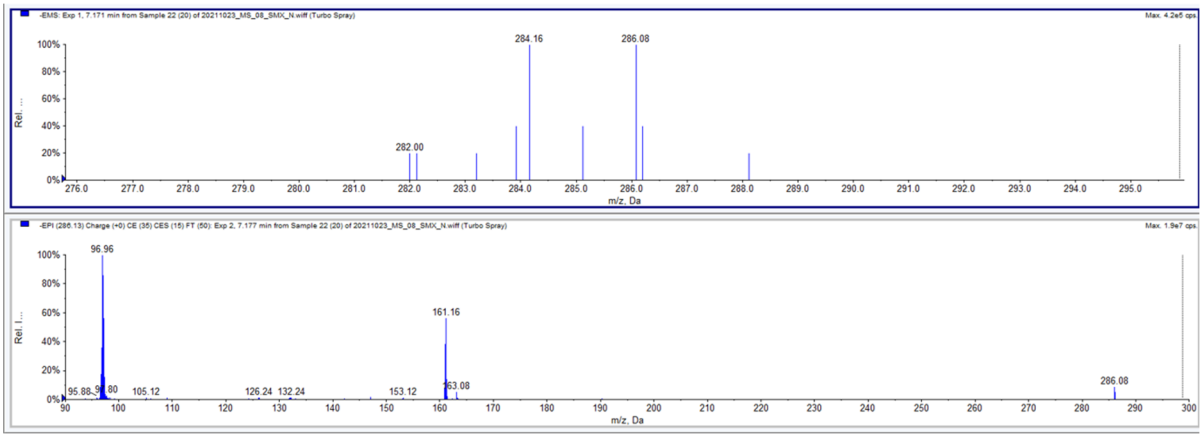

Figure S 12: Fragmentation pattern of OP282c, Rt: 6.7 min. A) ozone produced with technical oxygen ($^{16}O_2$), B) ozone produced with 55% $^{18}O_2$, C) ozone produced with 74% $^{18}O_2$

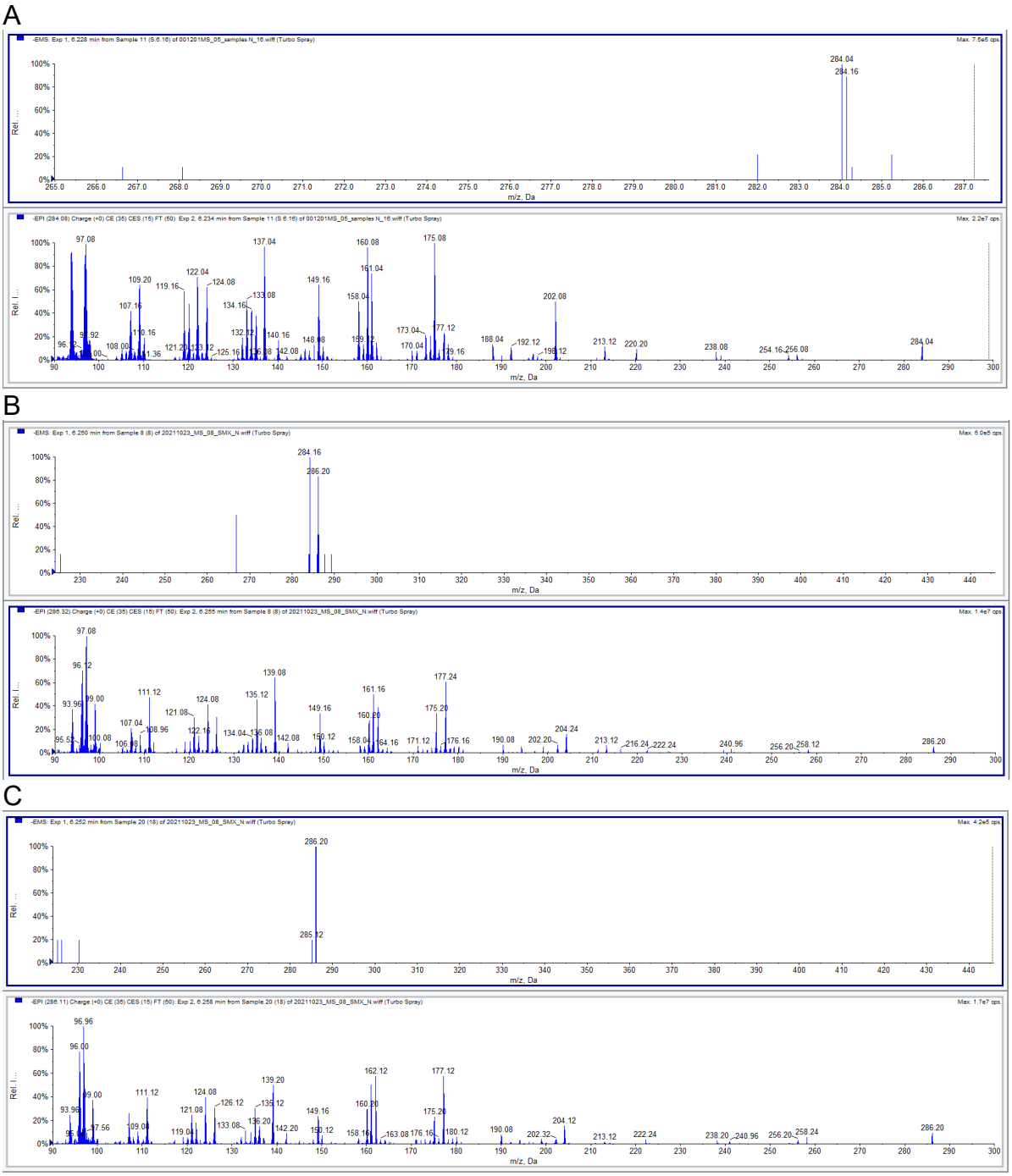

Figure S 13: Fragmentation pattern of OP284, Rt: 6.2 min. A) ozone produced with technical oxygen ($^{16}O_2$), B) ozone produced with 55% $^{18}O_2$, C) ozone produced with 74% $^{18}O_2$